Palaeogeography, Palaeoclimatology, Palaeoecology 639 (2024) 112087

Contents lists available at ScienceDirect

Palaeogeography, Palaeoclimatology, Palaeoecology

journal homepage: www.elsevier.com/locate/palaeo

Mid-Pleistocene Transition at a shallowing shelf: Tectonic and eustatic forcings in the paleoenvironment of the Enza section, Northern Apennines mountain front

Rossella Capozzi [a,*], Vincenzo Picotti [b,*], Valentina Alice Bracchi [c], Francesca Caridi [d], Anna Sabbatini [d], Marco Taviani [e,f], Stefano Bernasconi [b], Alessandra Negri [d]

[a] Department of Biological, Geological and Environmental Sciences, University of Bologna, Via Zamboni 67, 40126 Bologna, Italy
[b] ETH Department of Earth Sciences, Sonneggstrasse, 5 8092 Zürich (CH), Switzerland
[c] Department of Earth and Environmental Sciences, University of Milano-Bicocca, Piazza della Scienza 4, 20126 Milan, Italy
[d] Department of Life and Environmental Science, Polytechnic University of Marche, Via Brecce Bianche, 60131 Ancona, Italy
[e] Institute of Marine Sciences, Italian National Research Council (ISMAR-CNR), Via Gobetti 101, 40129 Bologna, Italy
[f] Stazione Zoologica 'Anton Dohrn', Napoli, Villa Comunale, Italy

ARTICLE INFO

Editor: M Elliot

Keywords:
Mid Pleistocene Transition
Sedimentology
Paleoecology
Marine isotopic stages
Argille Azzurre Fm
Northern Apennines

ABSTRACT

We present an integrated sedimentological, paleontological and oxygen isotope stratigraphic study of a Pleistocene marine to coastal section at the Enza river, allowing to highlight the role of tectonics at the mountain front of the Northern Apennines and that of climate at the onset of the Mid Pleistocene Transition. Two main evolutive steps, separated by a pronounced angular unconformity, characterize the deposition of the studied marine sedimentary succession ranging between 1.73 and 1.071 Ma. The lower part of the section shows a continuous outer shelf sedimentation, whereas the post unconformity sedimentation shows cyclothemes, documenting a progressive shallowing of the bathymetry. These are linked to enhanced eustatic oscillations leading to increasing amplitude of the transgressive-regressive cycles. The new $\delta^{18}O$ data allowed correlating the last 14 m underneath the unconformity to the MIS 49 to 45, improving our understanding of the time duration of the sedimentary gap, estimated around 140 ka. This is primarily associated with the growth of the Quattro Castella thrust ramp anticline, when a deeper mid-crustal thrust co-occurred, causing an increased deformation and tilting rate. The consequent change in morphotectonic setting strongly impacted the environment and ecosystem of this Early Pleistocene shelf. Starting at about 1.25 Ma, the section records an increasing riverine detritus, competing with the shore-parallel shelfal sediment dynamics. In a frame of increasing slope of the Northern Apennines topography, this enhanced fluvial activity might correlate with the increasing amplitude of climate oscillations during the Mid Pleistocene Transition, as recognized in other Mediterranean settings. This is recorded by a cyclothemic deposition, linked to eustatic oscillations.

1. Introduction

The Mid-Pleistocene Transition (MPT) is the interval of the Pleistocene in between ca 1250 and 750 ka when the Earth's climatic cycles changed in frequency and amplitude, passing from a dominant 40 to around 100 ka (e.g., Clark et al., 2006). Although there is no consensus about the ultimate causes of this ice age intensification, several mechanisms and atmosphere– bio/hydrosphere feedback have been discussed (e.g., Hönisch et al., 2009; Chalk et al., 2017; Berends et al., 2021; Herbert, 2023;), including the role of volcanism (e.g., Wang and Pierce, 2023). The effects of the MPT on the sedimentary systems, however, have been only recently addressed, mostly analyzing shelf deposits and their transgressive/regressive (T/R) cycles, such as in NE Australia (Ellerton et al., 2022) or in the South China Sea (Liu et al., 2022). Another study documents the intensified flushing of the oceanic canyons during the MPT, associated with increasing effects of eustatic drawdowns (Allin et al., 2017). Regarding the Mediterranean basin, the consequences of the MPT have not been analyzed, except for a pioneering work in the Crotone basin of Southern Italy (Massari et al., 1999). Taking advantage of the good exposures and available bio- and

* Corresponding authors.
E-mail addresses: rossella.capozzi@unibo.it (R. Capozzi), vincenzo.picotti@erdw.ethz.ch (V. Picotti).

https://doi.org/10.1016/j.palaeo.2024.112087
Received 19 August 2023; Received in revised form 16 January 2024; Accepted 11 February 2024
Available online 13 February 2024

magneto stratigraphy at the Enza section in the Northern Apennines (Gunderson et al., 2014), in this study we describe the sedimentary evolution of a former Mediterranean shelf under the forcing of the eustatic oscillations across the onset of the MPT. This succession is particularly intriguing since it also allows to infer the role of growing tectonic structures too. In the following, we will discuss how both the paleoenvironmental and structural evolution of the Northern Apennines mountain front may help constraining the role of MPT in that shelf depositional setting.

The present study focuses on the lower 142 m of the Enza River section of Gunderson et al. (2014), a Pleistocene marine section in the Emilia Romagna region of Italy (Fig. 1). Incised in the foothills of S. Polo d'Enza by the Enza River, a tributary of the Po River, the section provides an excellent exposure of the Pleistocene *Argille Azzurre* Fm, consisting of marine blue-grey muds and intervening sand bodies, overlain by marine transitional (*Sabbie Gialle* Formation) to continental deposits (Iaccarino and Monegatti, 1996; Gunderson et al., 2014).

Since long, the section is known for its paleontological richness, especially mollusks (Fornaciari et al., 1997), other invertebrates (Borghi, 2021), and carpological remains (Martinetto et al., 2015). Its fame, however, is linked to the presence of a spectacular record of former hydrocarbon seepage onto the seafloor, in the form of chimneys and other methane-derived carbonates (Blumenberg et al., 2015; Capozzi et al., 2015, 2017; Viola et al., 2015). As documented by decades of observations, the quality of the Enza exposure varies considerably over time in response to the river dynamics, and currently not much is visible of some of its most conspicuous and distinctive elements, like the palisade field of the hydrocarbon plumbing system or the rhodolith bed (see below). At the time of the deposition of the Enza succession, the former coastline was located to the South, prograding towards the present geographic location of the Enza section. The shelf was very likely narrow and inclined, as part of the external fold and thrust deformation of the foredeep basin, including those structures now buried under the Po Plain (Oppo et al., 2015) (Fig. 2). The *Argille Azzurre* Fm is the marine Plio-

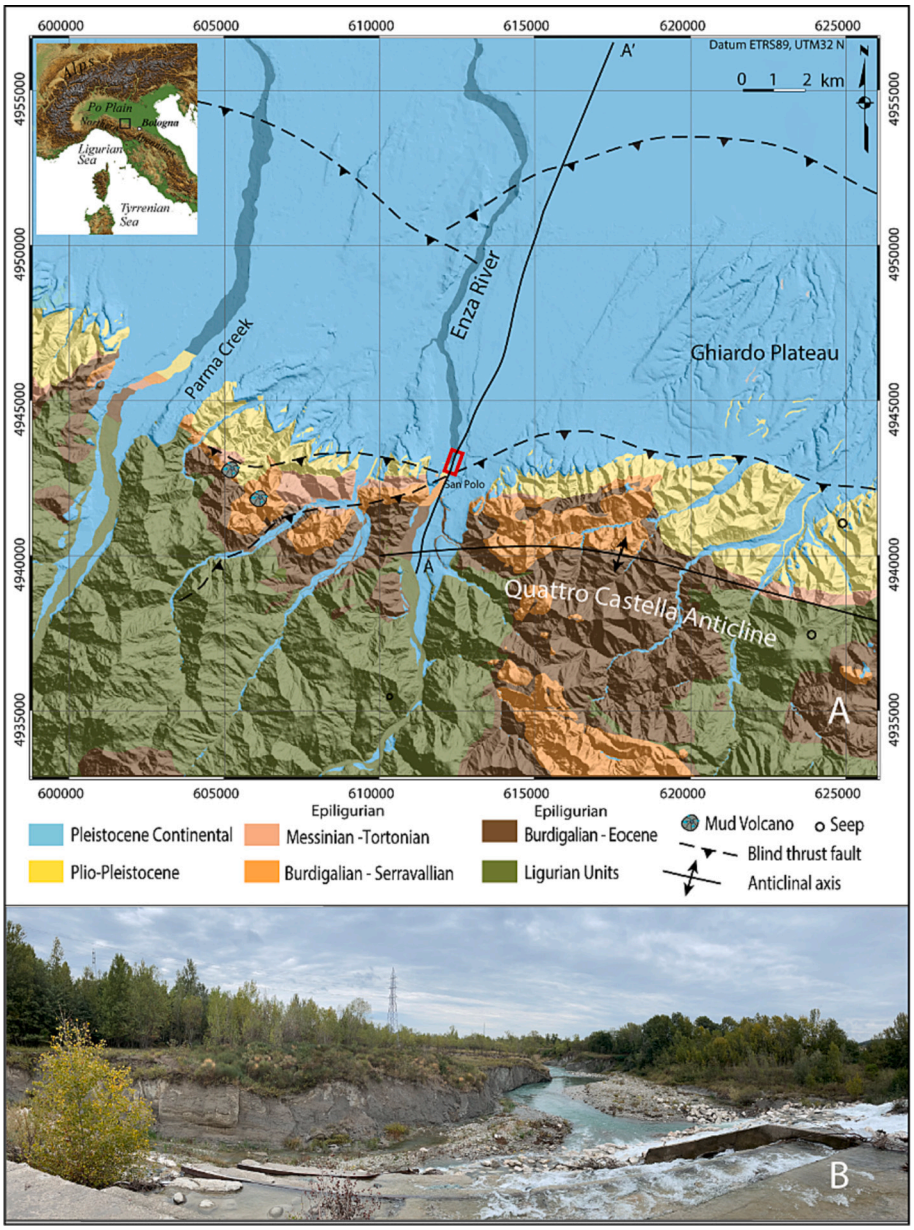

Fig. 1. A) Geologic map of the studied area; the red box indicates the studied section at the northern Apennine foothills. B) A view of the Enza River downstream of the check dam at S. Polo d'Enza, showing the sampled section. (For interpretation of the references to colour in this figure legend, the reader is referred to the web version of this article.)

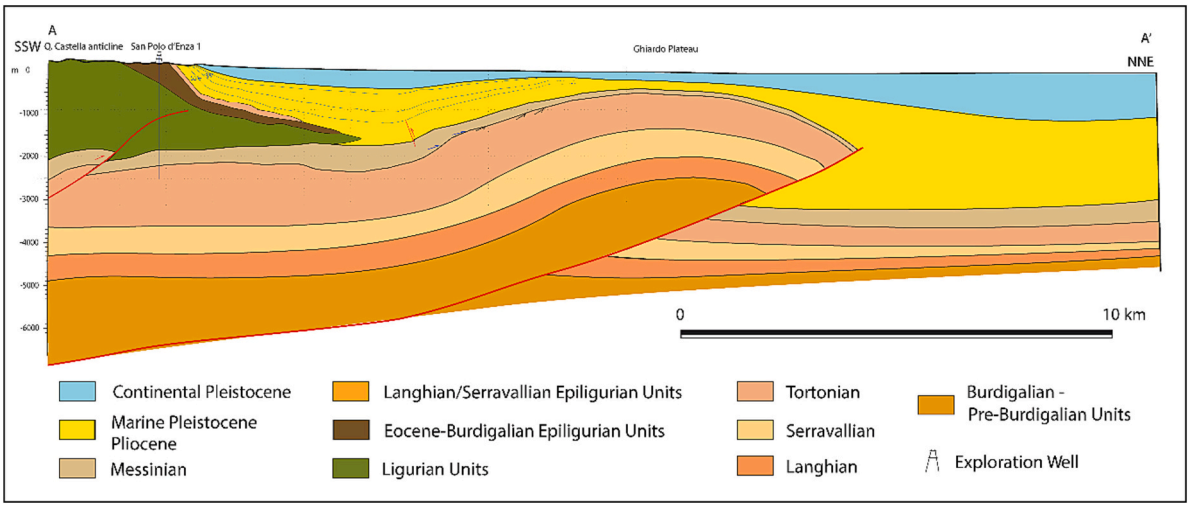

Fig. 2. Cross-sections along dip of the Northern Apennines mountain front in the studied area (see Fig. 1 for location). Reconstruction of the geological setting across the mountain front and the Ghiardo Plateau. Frontal ramps buried in the Po Plain are evidenced in red. (For interpretation of the references to colour in this figure legend, the reader is referred to the web version of this article.)

Pleistocene succession that extensively outcrops at the foothills of the northern Apennines, firstly described by Leonardo da Vinci (1506–1510), who coined this name. Brocchi (1814) divided the whole sedimentary succession in two members: a lower pelitic (*Argille Azzurre* Fm) unit and a sandy upper (*Sabbie Gialle* Fm) unit that he referred to the Astian (Early Pleistocene). This subdivision correctly describes the major variation of the deposition that records the transition to a coastal environment, during the uplift of the Apennine foothills. The *Argille Azzurre* Fm encompasses the time interval corresponding to the onset of the Arctic ice sheet (Berger and Loutre, 2000), that determined the transition to a markedly more rigid climate, and during which the magnitude of temperature and eustatic fluctuations became higher (Amorosi et al., 1999; Gibbard and Head, 2020).

The scope of our study is to unravel the role of the MPT in controlling the stratigraphic architecture and the paleoenvironment of marine shelf deposits, in a setting strongly influenced by the compressive deformation at the mountain front of the Northern Apennines (Figs. 1, 2). The study sheds light on the global control on the stratigraphic architecture at the onset of the MPT, thus offering a larger scale prediction tool for the correlation of coeval shelf successions.

2. Geological framework

The northern Apennines are an active fold-and-thrust belt developing since the Oligocene due to subduction of Adria under European-derived microplates, such as Corsica-Sardinia block (e.g., Molli, 2008). The studied sector of the Northern Apennines shows the wedge-shaped closure of the Ligurian Nappe, which is formed by the Jurassic-Eocene oceanic wedge, thrusted over the Miocene foredeep successions, and covered by the wedge-top basins of the Epiligurian Units (Figs. 1, 2) (Zattin et al., 2002).

In this compressive framework, the Plio-Pleistocene uplift of the chain led to the shallowing of the marine environments, as documented by the successions outcropping along the foothills (e.g., Gunderson et al., 2014). This process eventually led to continental deposition and the subsequent filling of the Apennine foreland basin in the Po Plain (e.g., Ghielmi et al., 2013). The mountain front of the Northern Apennines was established during the Pleistocene as a nearly rectilinear WNW-oriented feature (PTF of Boccaletti et al., 1985), separating the Apennines mountain belt from the Po Plain, i.e. the remnant of the foreland basin. The interpretation of the mountain front as deep mid-crustal thrust ramp, initially suggested by Picotti and Pazzaglia, (2008), was proven by seismics and seismological studies (e.g., Ponziani et al., 1995; Calderoni et al., 2009) and tectonic modelling of the growing stratigraphy on the Plio-Pleistocene of the foothills (Gunderson et al., 2013). The latter authors described the observed divergent geometry of the stratigraphy at the mountain front with a combination, occurring between 1.8 and 1 Ma of waning upper crustal and waxing mid-crustal thrusts, the latter forming the Emilia Mountain Front (EMF of Gunderson et al., 2013).

3. Material and methods

3.1. Lithostratigraphy

The portion of the Enza River section here considered (Fig. 1) refers to the lower 142 m of the section described by Gunderson et al. (2014). This lower part has been measured and sampled for a detailed lithostratigraphic reconstruction during multiple field surveys. In fact, river erosion has exposed or modified outcrops and new observations and measures have revealed lateral variations. The reconstructed stratigraphic section includes the stacking of the main lithofacies observed and measured along the riverbed, and their correlation along both the riversides.

3.2. Grain size analysis

As many as 169 samples (each 8 cm^3) were dried at 50 °C for 72 h, then weighed and wet sieved through a 62-μm American Society for Testing and Materials (A.S.T.M) sieve. The weight of the sandy fraction was later calculated as a percentage of the total weight. To characterize the sandy and bioclastic bodies in the upper part of the section some selected samples were freeze dried and then analyzed with a Malvern Master Sizer 3000 to obtain grain size distribution and the statistical parameters (sorting, kurtosis, skewness).

3.3. Foraminifera

In the first 128 m of the *Argille Azzurre* Fm, 45 samples (each 8 cm^3) were collected and processed for foraminiferal analyses (stratigraphic height shown in table S1). Preparation of fossil samples followed a standard technique. All samples were dried at 50 °C for 72 h and weighted. Then they were re-hydrated with distilled water and washed over a 63 μm sieve. Quantitative and qualitative analyses of benthic foraminifera were performed on the >150 μm size fraction of all samples. All the benthic specimens present in the residue were identified

according to the generic classification of Loeblich and Tappan (1987). The species identification was based mainly on previous studies on the Adriatic basin (Agip, 1982; Jorissen, 1987; Morigi et al., 2005). The foraminiferal diversity was calculated using relative abundances of all species. Specifically, species richness (S) was measured as the number of species.

3.4. Macrofossils

Macrofossils are abundant but unevenly distributed in the entire section. In order of relative abundance, skeletal biosomes and bioclasts of the following taxonomic macropaleontological groups were positively identified: Mollusca, Bryozoa, Scleractinia, Annelida (Serpulidae), Echinodermata, Decapoda, Brachiopoda, Pisces. Fossils were collected in bulk samples to identify smaller taxa, and as seen for taxa larger than 1 cm. Because of the overwhelming abundance of Mollusca over other groups, the eco-biostratigraphic and paleoecological inferences are by large based upon this Phylum.

3.5. Coralline red algae

Coralline red algae form two distinct horizons of densely packed rhodoliths at 66.4 and 70 m, separated by planar laminated medium-sized sandstones in which rhodoliths are sparse. The horizon has been measured and rhodoliths ($n = 16$) have been classified based on their morphology (boxwork, praline or branches) according to Basso (1998). The rhodolith shape follows Bosence (1983) scheme by measuring the long (a), intermediate (b) and short (c) axes of all rhodoliths. In addition, at the base of the outcrops, methane-derived carbonate chimneys encrusted by calcareous algae occur and therefore two additional samples have been collected. All samples have been sliced for thin sections, to investigate the occurrence of nucleus and the inner structures (rhodoliths), and for non-geniculate red algae description and identification. The identification follows the biological nomenclature of Woelkerling (1988), as revised by several subsequent contributions (Bressan, 2003; Irvine and Chamberlain, 1994), and its application to paleontology (Braga, 2003; Hrabovskỳ et al., 2016; Pezzolesi et al., 2019). Algal taxonomy follows Algaebase (Guiry and Guiry, 2020).

3.6. Stable isotope geochemistry

Stable oxygen and carbon isotope analysis was performed on *Cibicides refulgens* found on the first 64.8 m below the unconformity. Five to ten specimens of *C. refulgens* were picked under the microscope in the size fraction of 250 to 350 μm and stored in a plastic vial. The isotopic composition was measured using a GasBench II coupled to a Delta V mass spectrometer (both Thermo Fischer Scientific, Bremen, Germany) as described in Breitenbach and Bernasconi (2011). About 100 μg of powdered samples were placed in vacutainers, flushed with helium, and were reacted with 5 drops of 104% phosphoric acid at 70 °C. In batch of 70 samples instrument was calibrated with the internal standards MS2 ($\delta^{13}C = +2.13‰$, $\delta\ ^{18}O = -1.81‰$) and ETH-4 ($\delta^{13}C = -10.19‰$, $\delta^{18}O = -18.71‰$), which are calibrated to the international reference materials NBS 19 ($\delta^{13}C = +1.95‰$, $\delta\ ^{18}O = -2.2‰$) and NBS 18 ($\delta^{13}C = -5.01‰$, $\delta^{18}O = -23.00‰$; Bernasconi et al., 2018). Values are reported in the conventional delta notation with respect to VPDB.

4. Results

The entire section under scrutiny is of Pleistocene age, as convincingly documented by biostratigraphic and magnetostratigraphic data (Gunderson et al., 2014; this study). The precise age assessment, however, is not easy, since a large part of the section is represented by relatively shallow marine deposits, where planktic foraminifera and calcareous nannofossils are missing or poorly preserved, except for the very base of the section showing the FO of *Gephyrocapsa oceanica* (1.73 Ma, Raffi et al., 2006). Regarding benthic organisms of ascertained eco-biostratigraphic value, only the index-fossil *Arctica islandica* does occur at basal levels and near-terminal part of the section (Fornaciari et al., 1997, unpublished Master Thesis, University of Parma; Gunderson et al., 2014; this study), confirming the Pleistocene age for the sequence, since its presence in the Mediterranean relates to cold times of the entire Pleistocene (Malatesta and Zarlenga, 1988; Taviani et al., 2011).

4.1. Lithostratigraphy

Along the Enza River, the stratigraphic succession shows a marine sedimentary record where the *Argille Azzurre* Fm is separated into two main intervals by a prominent unconformity (Gunderson et al., 2014; Oppo et al., 2015). The basal interval consists of ca. 66.4 m of mudstones deposited on the shelf below the storm wave-base (*Argille Azzurre* outer shelf in Fig. 3) that shows a very low sand content (Fig. 4). In detail, the lower 15 m consist of dark grey mudstones, locally rich in fossils, finely bedded for the presence of silty-sandy horizons (Figs. 3, 4). The remaining succession, up to 64 m, which bears several methane-derived pipe-like carbonate chimneys and lens shaped concretions between 30 and 65 m (Gunderson et al., 2014; Oppo et al., 2015), consists of poorly bedded to massive grey to blue-grey mudstones, again punctuated by finer sandy horizons. Locally, the massive appearance is enhanced by the joint effects of bioturbation and gas migration that impart a strong mottling. The gas-migration occurs mostly through fractures and pipe-shaped conduits that lead to the Methane-Derived carbonate Concretions (MDC) in the shape of chimneys and, towards the top, of layer parallel slabs (Oppo et al., 2015; Viola et al., 2015; Capozzi et al., 2017). This mudstone interval is topped by the angular unconformity that marks the abrupt transition to a shallow water inner shelf to shore, which is the second half of the studied succession (Fig. 3).

The angular unconformity along the section of Fig. 3 at 66.4 m is carved onto the mudstones and the methane-derived carbonate slabs intensely bored by infralittoral lithodomes (*Lithophaga lithophaga*). Immediately above the unconformity, a very distinct composite bed calciruditic to calcarenitic occurs (Gunderson et al., 2014), dominated by calcareous red algae, forming rhodoliths that locally coat fluvial pebbles, encrustations of bryozoans, and small patches of the coral *Cladocora caespitosa*. This 2.5 m thick unit consists of gravels floating in a coarse sandy matrix that includes fragments of the underlying carbonate concretions, with 2 to 8 cm large rhodoliths (Rhodolith bed in Fig. 3). Locally, black sulphidic concretions suggest the occurrence of methane seepages through this horizon. The rhodoliths tend to disappear upwards and the calcirudite/calcarenite bed is finally capped by a 1.3 m thick pelitic bed. The whole interval is thicker towards the riverbed (east), where measuring and sampling have been done (Fig. 3). A second downcutting erosional surface cuts the underlying succession towards the west. It is covered by a coarse-grained bed with thickness varying from 2.6 to 6 m moving East. In its proximal part, this bed consists of a pebble layer that passes eastward to planar laminated medium-sized arenites, marked by aligned bioclasts. Above the arenites, a 40 cm thick fining up massive sandy-siltstones grades to mudstones, in turn covered by 60 cm sand-sized well laminated bioclastic sandstones rich in mollusks and rhodalgal nodules (Channel in Figs. 3). This coarse-bedded interval is abruptly covered by around 2.5 m thick coarsening-up mudstones/siltstones with faint lamination. An interval of around 5 m of sandstones follows, showing dm-scale beds, with internal cross-lamination, ending at 82 m of the measured section (Mouth bar crest in Fig. 3). The top of this last unit is marked by a ten cm-thick bed, mostly consisting of *Ditrupa arietina* in a sandy matrix (Fornaciari et al., 1997, unpublished Master thesis, University of Parma). Above the *Ditrupa* bed, a sharp transition to an about 11 m-thick intervals of mudstones, rich in mollusks, occurs (Prodelta in Fig. 3). It passes gradually up section, to siltstones and sandstones arranged in three massive beds of 2–3 m in thickness, with faint internal lamination (Fig. 3). The overlying 5–6 m of succession consist of laminae formed by coupled cm-

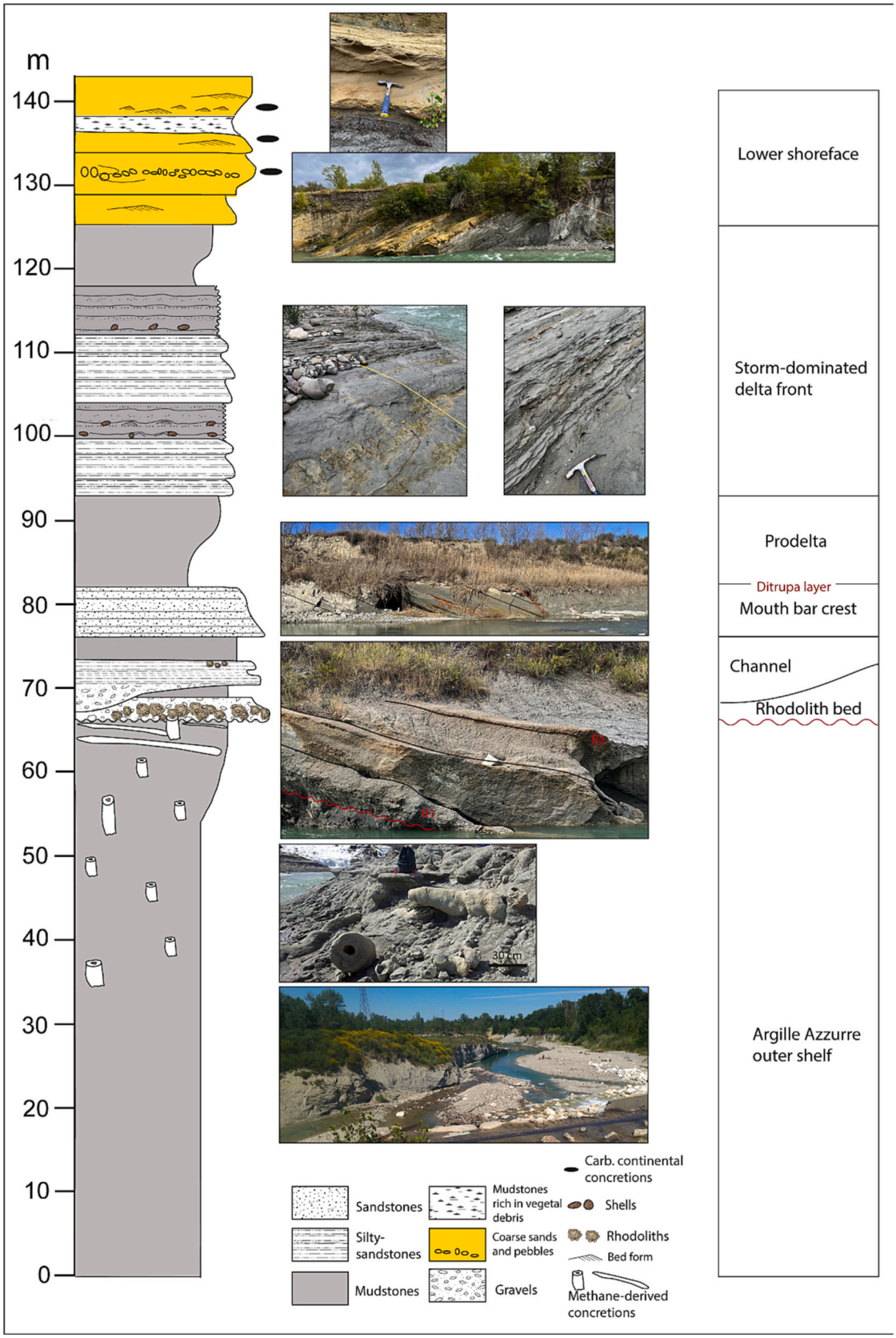

Fig. 3. Stratigraphic section of the *Argille Azzurre* Fm and base of *Sabbie Gialle* Fm, measured along the Enza River. The lithofacies stacking pattern is matched with outcrop pictures and the interpretation of depositional environments. See text for explanation.

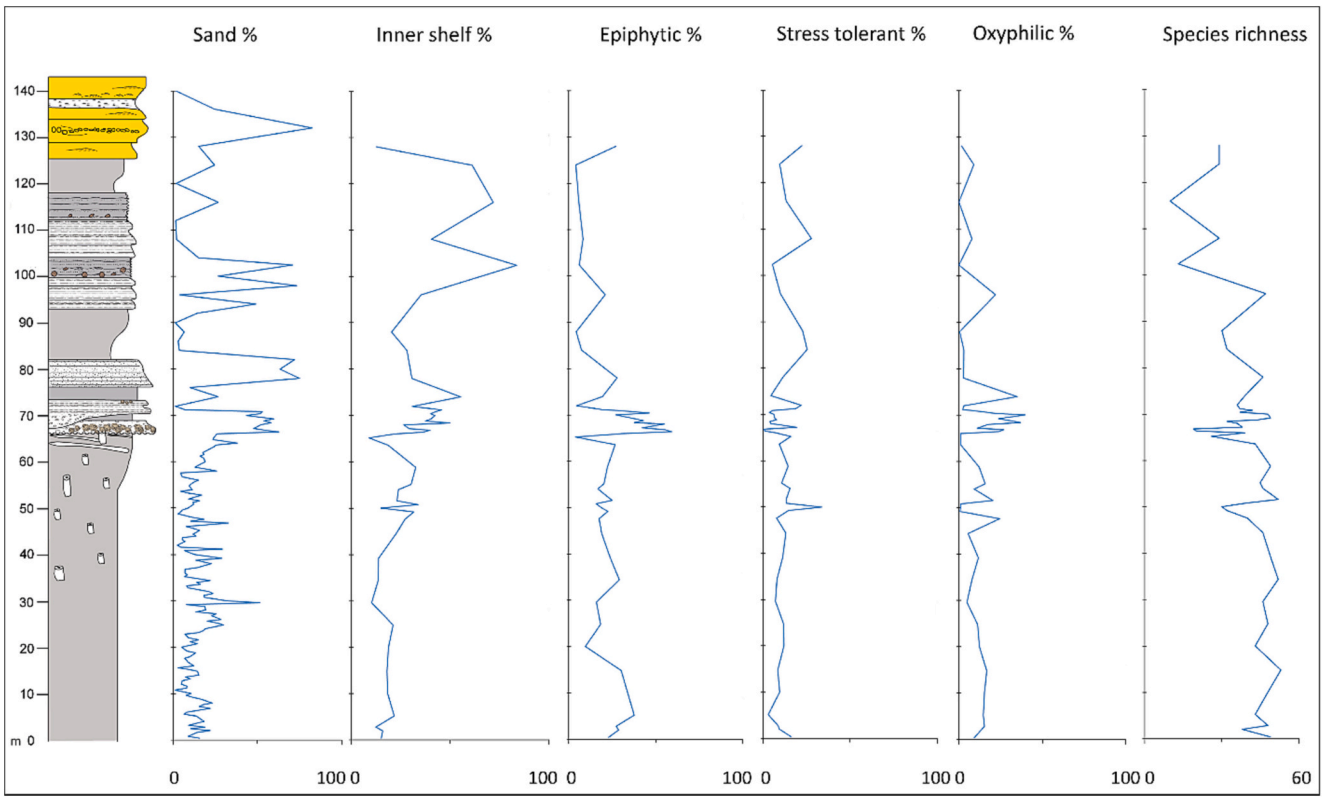

Fig. 4. Benthic foraminifera assemblage. The distributions show the fluctuations across the section of the four major groups recognized (inner shelf, epiphytic, stress tolerant and oxyphilic), compared with sand fraction percentage and species richness.

thick coarse sands, with wavy to cross laminations (hummocky to ripples) and basal lags with vegetal debris and marked by disarticulated, aligned, and at times blackened bivalves, including *Arctica islandica*, likely reworked by storm currents, and draped by mud (e.g., Jelby et al., 2020). This interval of tripartite sandstones and cross-laminated beds is repeated twice up to 118 m of the section (Storm-dominated delta front in Fig. 3). A massive mudstone interval of about 7 m covers those two cycles. At 125 m of the measured section (Fig. 3), well-bedded grey sands occur, upward passing to yellow sands. These sands, 10 m in thickness, are arranged in a stacking pattern showing at the base 3 m of medium-sized sands, with internal parallel laminations. The central interval, at 128 m, shows a significant sharp base marked by coarse sands with minor pebbles, and relevant carbonate concretions formed during subaerial emersion and meteoric groundwater circulation (Pizzati et al., 2018)(Fig. 3). Similar concretions, locally including Fe-oxides, occur at 131–132, 136–137 and 139–140 m (Pizzati et al., 2018). The final part of the measured section shows coarse, cross-bedded yellow sands ending at 142 m from the base of the section (Lower shoreface in Fig. 3). The top of the measured section, further passing to the *Sabbie Gialle* Fm not included in this study, consists of about 2 m finely bedded sands, showing ripples in a medium cross laminated stratification, locally truncated by planar erosional surfaces. They alternate with organic-rich dark-grey mudstones, rich in plant debris (Fig. 3).

4.2. Foraminifera

The assemblage consists of benthic with very rare planktonic foraminiferal taxa. A total of 118 benthic species belonging to 65 genera have been identified in the 45 samples studied. The number of benthic specimens counted varies from 53 to 459. The species richness ranges from 10 to 53 species per sample (Fig. 4; table S1), with the highest values recorded in the lower part of the succession.

Based on the ecological preferences of the different taxa, we can distinguish four main groups (Fig. 4). The first consists of inner-shelf species typically found at depths ranging from 0 to 50 m. These species are often associated with coastal environments characterized by coarser sediment and influenced by riverine input (Jorissen, 1987; Gupta and Machain-Castillo, 1993; Mendes et al., 2004): *Ammonia beccarii*, *A. inflata*, *A. parkinsoniana*, *Aubignyna perlucida*, *Elphidium advenum*, *E. decipiens*, *Porosononion granosum*, *Quinqueloculina* group, *Triloculina* group and *Textularia* group. To this cluster belongs the *Quinqueloculina* species, including the species *Q. schlumbergeri* and specimens belonging to *Quinqueloculina* sp.; *Triloculina* species, as *T. gibba* and specimens belonging to *Triloculina* sp.; finally, the agglutinated group of *Textularia* includes *T. agglutinans*, *T. conica* and *T. simplex*.

The second cluster represents epiphytic species, which are diverse and often specialized taxa growing on the microalgal, macrophytes and bacterial biofilms (Mojtahid et al., 2011; Schweizer et al., 2022), which need sandy substrate and a strong hydrodynamic energy (Tomadin et al., 1984; Langer, 1993; Mateu-Vicens et al., 2010; Manda et al., 2020; Rossbach et al., 2021). In this cluster we consider *Adelosina* group (*A. longirostra*, *Adelosina* sp.), *Asterigerinata mamilla, Buccella frigida, Cibicides* group *(C. refulgens, C. pachyderma)* and *Cibicidoides* group (*C. wuellerstorfi, C. pseudoungerianus, C. robertsonianus, C. ungerianus, C. variabilis)* together with *Elphidium crispum, E. macellum, Gavelinopsis* sp., *Lobatula lobatula, Neoconorbina* sp., *Planulina* sp., *Planorbulina mediterranensis, Reussella spinulosa, Rosalina globularis, Miliolinella* sp.

The third group comprises stress tolerant species commonly found in the inner to outer shelf regions. Stress tolerant foraminifera exhibit a rapid response to environmental changes, allowing them to thrive in disturbed or stressed ecosystems. These species are often characterized by their ability to tolerate low oxygen levels, high organic matter concentrations, and other adverse conditions (Bernhard et al., 2018; Fontanier et al., 2008; Goineau et al., 2011; Mojtahid et al., 2009; Wollenburg et al., 1998). It includes *Ammonia tepida, Bulimina* group (including *B. aculeata, B. denudata, B. elongata, B. inflata, B. marginata, B.*

striata costata), *Buliminella elegans*, *Haynesina* sp., *Melonis padanus, M. pompiliolides, Nonionella opima, Nonionoides turgidus*, and *Valvulineria bradyana.*

The fourth group, known as "oxyphilic," encompasses species that have a specific requirement for high oxygen concentrations. These foraminiferal species thrive in environments characterized by well-oxygenated bottom conditions. They are sensitive to low oxygen levels and tend to be more prevalent in areas with good water circulation and sufficient oxygen supply (Sen Gupta and Sen Gupta, 2003). It includes *Cibicidoides mundulus*, *Oridorsalis umbonatus* and miliolids, among them *Adelosina*, *Quinqueloculina*, *Sigmoilina*, *Sigmoilinita*, *Spirillina*, *Spiroloculina*, *Pyrgo* and *Triloculina.*

The first 65 m of the section (Fig. 4) exhibits inner shelf species below 40%, and the abundance of epiphytic species is also not high, indicating a depth exceeding 50 m. Starting from 65.2 m the benthic foraminiferal taxa, in particular the epiphytic species *E. crispum* and *A. mamilla* (see Fig. 4 and table S1), show a significant increase that correlates with the increase in sandy fraction. Soon after, at 66.4 m the erosional unconformity ends the deposition, which will eventually recover with the rhodalgal colonization.

The upper part of the section, from 74 to 128 m, shows a higher variability and can be further subdivided into two intervals. A first one, up to 94 m, is characterized by low abundance of inner shelf and epiphytic groups, coupled to an increase of stress tolerant species represented mainly by species belonging to the *Bulimina* group, possibly indicating organic matter enrichment, and associated with fine-grained sediments (Fig. 4). Between 94 and 128 m, where the sand content increases, the assemblage shows a significant increase of the inner shelf species that mirror the drop of epiphytic species, while stress tolerant taxa fluctuate. In this upper part, species as *A. beccarii*, *A. parkinsoniana*, *A. perlucida*, *E. decipiens* and *P. granosum* and *Textularia* group adapted and/or tolerant to high nutrient riverine input are abundant (see Table S1).

4.3. Rhodoliths

Rhodoliths characterize a distinct horizon between 66.4 and ca 68 m, whereas between 70 and 73 m are mainly reworked within medium-sized arenites and show very localized small pockets of re-colonization (Fig. 5). The first densely packed rhodolith layer (R1 in Fig. 5) forms a rhodolith bed of at least 50 cm in thickness and several meters of lateral continuity, therefore considered as autochthonous (Table 1), whereas in the upper part they are sparser. Rhodoliths are of boxwork and praline morphotype (Table 1), with a sub-spheroidal to spheroidal shape. Specimens are compact, and do not show evident macrocavities or, when present, they are filled by sediment. For this reason, the specimens identified as boxwork are very similar to praline, but being multispecific, they formally correspond to this category. Moreover, pralines generally show a low degree of branching. Rhodolith size varies from Enza 3_4 (long axis = 6.6 cm, short axis = 4.3 cm) to Enza 4_2 (long axis = 2.8 cm, short axis = 2.4 cm) (Table 1). Rhodoliths show both biogenic nuclei as old algal nodules (Enza 1_2, 1_4, 2_4, 3_1, 3_3, 4_3), or other skeletal nucleus (Enza 1_3, 4_4), or lithic (micrite, Enza 2_2, 4_2), whereas six of them do not show evident nucleus (Table 1).

Identification was challenging because of the bad preservation of specimens. The genus *Lithothamnion* is the most abundant, whereas *Lithophyllum,* the genus *Mesophyllum* and unidentified *Lithophylloidea* occur, but mostly in the inner part (nucleus) of some rhodoliths and as very small fragments (Table 1). In addition, the genus *Titanoderma* has been often recognized (Table 1) thanks to the typical palisade cells. On the contrary, samples Enza 2_2 and 3_2 (Fig. 5) are monospecific *Lithophyllum racemus* and show a typical globular shape. The basal chimney encrustation consists of a very thin layer of exclusively *Titanoderma* sp. (Table 1).

4.4. Mollusks and other macrofossils

The lower 60 m of the section, the *Argille Azzurre* show frequent *Turritellina tricarinata*, *Corbula gibba* and *Ditrupa arietina*. Between 20 m and 60 m a highly diverse epifaunal and infaunal macrofauna occurs (e.

Fig. 5. Outcrop showing the erosional surface at 66.4 m of the section (in red), the occurrence of the underlying methane-derived carbonates (circled in white) and the overlying succession with intervening rhodolith beds. The sampled interval includes a main horizon, indicated with R1, and the uppermost indicated with R2. Black lines indicate main bed sets with increasing thickness towards the riverbed. The R2 bed contains well-preserved rhodoliths within pockets, in a mostly reworked sediment. Some rhodoliths are shown in the pictures in the lower part of the figure and red arrows indicate the sampling location (see Table 1, list of samples). Rhodolith sample 1_2 belongs to the lower bed (R1), just above the unconformity; Rhodolith sample Enza 4_3 belongs to the upper bed (R2). Rhodolith samples 2_2 and 3_2 have been recovered in the coarse-grained interval between R1 and R2. (For interpretation of the references to colour in this figure legend, the reader is referred to the web version of this article.)

Table 1
Rhodoliths samples, with the indications of location along the stratigraphic log, morphotypes, type of nucleus, dimension and identified coralline species (for abundance). Na = not applicable; bp = bad preservation.

Location	Sample name	Morphotype	Nucleus	Axis			CCA species
				a (long)	b (interm.)	c (short)	
Chimneys	Enza_chimney_1	na	na	na	na	na	bp
	Enza_chimney_2	na	na	na	na	na	*Titanoderma* sp.
R1	Enza 1_1	boxwork	not evident	3.3	2.8	1.5	*Mesophyllum* sp., *Titanoderma* sp.
	Enza 1_2	boxwork	old algal nodule	4.7	4.3	4	*Lithothamnion* sp., Lithophylloidea *(*nucleus*)*
	Enza 1_3	boxwork	bryolite	4	3.7	3.1	bp
	Enza 1_4	praline	old algal nodule	4.6	4.3	3.4	Lithophylloidea (nucleus)
Inter layer	Enza 2_1	boxwork	not evident	2.6	2.5	2.4	*Lithophyllum* sp.; *Mesophyllum* sp.
	Enza 2_2	boxwork	micrite	3.5	3.2	3.2	*Mesophyllum* sp.; Lithophylloidea
	Enza 2_3	praline	not evident	3.4	2.7	2.2	*Lithophyllum racemus*
	Enza 2_4	boxwork	old algal nodule	3.6	3.2	3.1	*Lithothamnion* sp.; *Titanoderma* sp.; Lithophylloidea
	Enza 3_1	boxwork	old algal nodule	4	3.4	3	*Titanoderma* sp.; *Mesophyllum* sp.
	Enza 3_2	boxwork	not evident	3.2	2.2	2.1	*Lithophyllum racemus*
	Enza 3_3	boxwork	old algal nodule	3.5	3.4	3.1	*Lithothamnion* sp.; *Titanoderma* sp.; Lithophylloidea (nucleus)
	Enza 3_4	boxwork	no	6.6	5.7	4.3	bp
R2	Enza 4_1	boxwork	not evident	2.8	2.8	2.6	*Lithothamnion* sp.; Lithophylloidea (nucleus)
	Enza 4_2	praline	micrite	2.8	2.6	2.4	*Lithothamnion* sp.
	Enza 4_3	praline	old algal nodule	3.4	2.6	2.5	Lithophylloidea (nucleus)
	Enza 4_4	praline	skeletal	3	2.7	2.4	*Titanoderma* sp.

g., *Tritia prysmatica, Turricula dimidiata, Clavus sigmoideus, Trophonopsis squamulosus, Teretia anceps, Alvania puntura, Nucula placentina, Nuculana commutata, Amusium cristatum, Flabellum* sp.). The holoplanktic mollusks (e.g., the pteropod *Euclio pyramidata*) between ca. 30–60 m are usually associated to pelagic input within a deep shelfal environment. One noticeable characteristic is the patchy occurrence of oyster-vermetid serpulid build-ups at ca. 40 m, consisting of *Ostrea edulis*, *Petaloconchus intortus*. and *Serpula* sp. indicating times of lower sedimentation rates within an otherwise muddy-silted environment. Interestingly, some methanogenetic chimneys between 50 m and 60 m embed valves of *Aequipecten opercularis* and other shelfal pectinids. Overall, based upon the macropaleontological content, the whole interval was deposited in a shallowing-upwards middle-outer shelf setting with estimated paleodepths passing from ca. 80 to 30 m.

At the unconformity (66.4 m), infralittoral lithodome bivalve (*Lithophaga lithophaga*) occurs, boring loose slabs of methane-derived carbonates. Other bivalves (*Hiatella arctica*, *Petricola* sp.), as well, nestled those borings.

In the post-unconformity interval between 66.4 and 74 m, we have identified mollusks associated with algal/phanerogam habitats (e.g., *Tricolia* sp., *Jujubinus* sp., *Bittium* sp.), muddy unstable environments (*Turritellina tricarinata*, *Corbula gibba*, *Ditrupa arietina*), alternating with hard bottoms (*Bolma rugosa*, and the coral *Cladocora caespitosa*) and detrital bottoms (*Archimediella*, *Astarte fusca*, Pectinidae spp.).

In the interval 82–93 m, the mollusk assemblage documents the abundance of *Venus nux*, often articulated, together with *Nassarius solidula*, *Turritellina*-rich horizons and thin layers with abundant *Ditrupa arietina.* Within some thin sandy beds, a prevalence of bivalves (e.g., *Spisula subtruncata*, pectinids, tellinids, *Solecurtus* sp.,) and the gastropod *Aporrhais pespelecani* occur. In the upper part of this interval, *V. nux* is again very abundant, associated with *Glycymeris nummaria* and *Nassarius solidula.* After 93 m, a variety of bivalves occur, such as *Spisula subtruncata*, *Azorinus chamasolen*. A storm layer at 100 m consists of a lag of isoriented and convexity-up valves of *Arctica islandica*, together with *A. opercularis* and *V. nux*. A second layer at 115 m is also enriched in *Arctica* valves, associated with *Nucula* sp., *Glycymeris nummaria*, *Anomia ephippium*, *P. papillosum*, *V. nux*, *S. subtruncata*, and rare gastropods (Naticidae sp.). The layer at the top of the well-sorted sands (138 m) includes articulated *Chamelea gallina* bivalves.

5. Age model

The age model for the studied section relies on available data published in Gunderson et al. (2014), complemented with the new stable isotope data. At 1.6 m from the base of the section, the First Occurrence (FO) of *Gephyrocapsa oceanica* has been found, dated at 1730 ka by Raffi et al. (2006), whereas at 142.5 m, towards the top of the studied section, Gunderson et al. (2014) reported the base of the Jaramillo event, dated at 1071 ka (e.g., Gibbard and Head, 2020). The section is split into two parts by a prominent angular unconformity at 66.4 m, therefore making an interpolation of these two calibrated ages difficult and requiring more data near the unconformity. The $\delta^{18}O$ data on *Cibicides refulgens* (Fig. 6) provide these new constraints, allowing the correlation with the Medstack curve obtained by Wang et al. (2010), in turn matching well the Lisiecki and Raymo (2005) global stack. Between 50 and 64.8 m, three lighter negative $\delta^{18}O$ peaks are correlated for amplitude and frequency to MIS 49, 47 and 45, respectively aged 1471, 1429 and 1400 ka (Wang et al., 2010) (Fig. 6). From the analysis of the $\delta^{18}O$ curve, the pre-unconformity succession would include up to the negative peak of the MIS 44 (Fig. 6), 1385 ka according to Gibbard and Head, (2020). The time encompassed within the unconformity was proposed to be approximately around 140 ka, using the measured angular separation of 7°(Oppo et al., 2015). A discussion on the tectonic meaning of this angular unconformity is given in the next section. Adopting this estimation, the age of the post-unconformity recovery of deposition would be around 1245 ka. We noticed that this time span corresponds to a rise of the eustatic sea-level curve after a negative drawdown peaking at 1255 ka (MIS 38, see Miller et al., 2005; Gibbard and Head, 2020). The MIS 38 is one of the most important drawdowns of the sea-level in the studied interval 1730 to 1071 ka and is usually taken as the onset of the MPT (e.g., Berends et al., 2021; Herbert, 2023). The subsequent eustatic rise would then correlate with the rhodolithic bed at the base of the post-unconformity succession. Finally, the correlations of the minor unconformities atop the sand beds with the $\delta^{18}O$ curve in between 1245 and 1071 ka (Fig. 6) is tentative and not further constrained.

The pre-unconformity succession was deposited in a time span of 345 ka, with an average sedimentation rate for the *Argille Azzurre* Fm of 19 cm/ka, in a muddy outer shelf, as also reported by Gunderson et al. (2014). Within the discussed time frame of the post-unconformity succession, the sedimentation rate for this inner shelf to shore succession, 42 cm/ka is more than double than the pre-unconformity one. Given the shallow bathymetry of this sedimentary environment, the sedimentation rate corresponds near one to one to the subsidence rate.

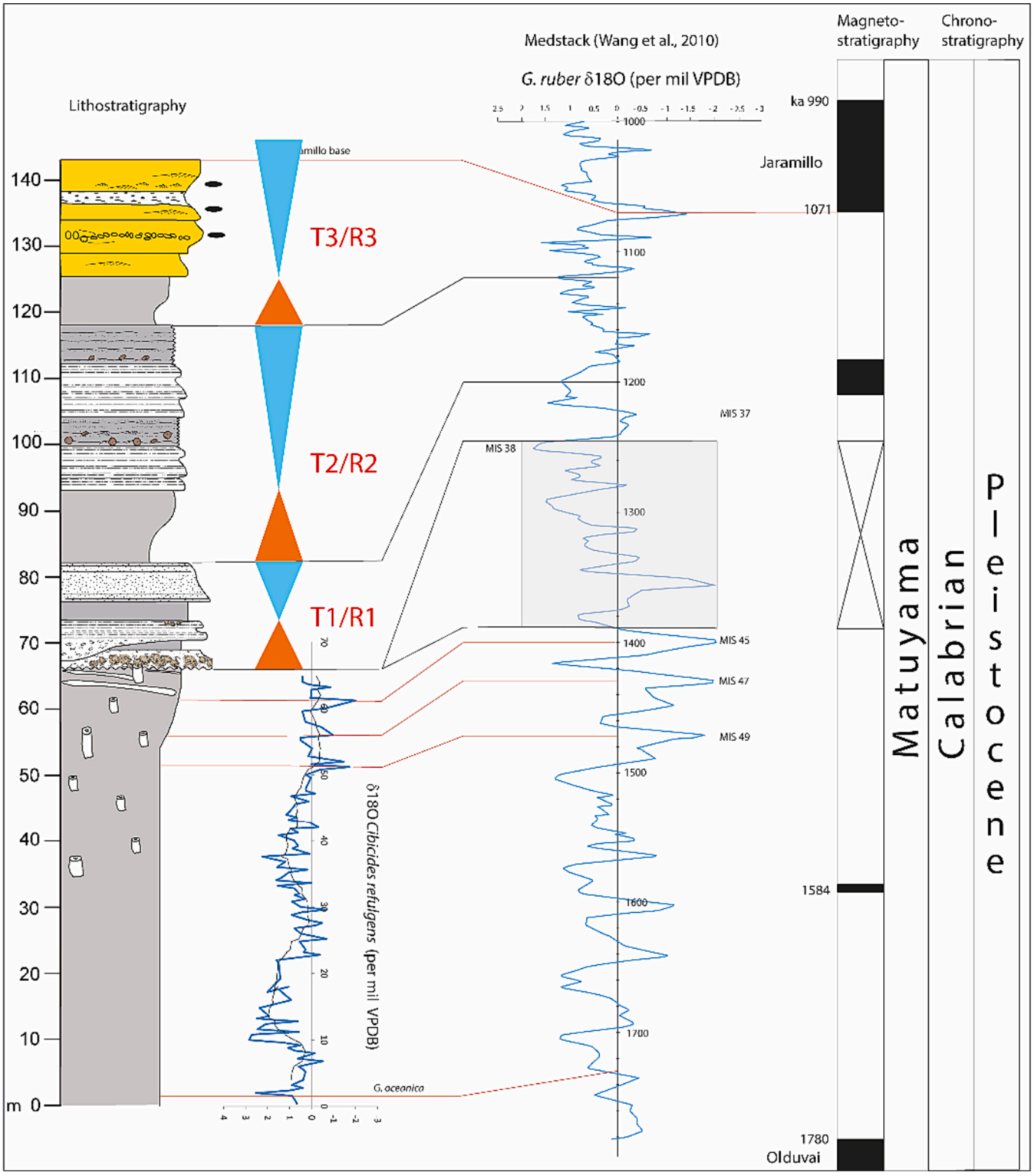

Fig. 6. Age model of the Enza River section. It is confined by the occurrence of the *Gephyrocapsa oceanica* at 1.6 m (1.73 Ma) and the base of the Jaramillo event at 142 m (1.071 Ma), (Gunderson et al., 2014). The $\delta^{18}O$ analysis on *Cibicides refulgens* (this study) includes isotopic stages 49 to 45 from 50 to 64.8 m. The section has been correlated with the Medstack (Wang et al., 2010). The shaded square indicates the stratigraphic hiatus occurring at the angular unconformity at 66.4 m (ca. 140 ka). The post-unconformity succession is arranged in three main cycles (T/R), correlated with the Medstack.

6. Discussion

In this section we will integrate the lithostratigraphic and paleontological data into a paleoenvironmental reconstruction, then discuss the effects of tectonic and eustatic forcings at the onset of the MPT on the sedimentary succession of the Enza section.

6.1. Paleoenvironmental reconstruction on the pre-unconformity outer shelf interval

The lower part of the section, extending until 66.4 m, displays poor bedding and a very low occurrence of the >63 μm grain fraction (Fig. 4). Additionally, the low abundance of inner shelf and epiphytic foraminiferal species further supports the interpretation of a relatively deep-water system, well below the storm wave base. The occurrence of a well-diversified micro- and macrofauna with prevailing species typical of outer shelf further strengthens this interpretation. The microfossil content is very diverse and consistent with a circalittoral muddy environment in an estimated bathymetric range between 70 and 100 m. At around 15 m of the section, a well-diversified microfauna occurs with relatively abundant (up to 35%) epiphytic species. Stress tolerant and oxyphilic species are generally not abundant and show antithetic fluctuations (Fig. 4). An evident peak of stress tolerant species (*M. padanus, M. pompiliolides* and *V. bradyana,* Table S1) is detected at around 50 m, corresponding to centimetric organic matter-rich layers, interbedded to the bioturbated sediment. Overall, the microfossil assemblage suggests a well-oxygenated, stable algal meadow of outer shelf on a muddy substrate with available nutrients (Fig. 4).

We also observe in this interval the occurrence of epiphytic taxa (*A. mamilla*, *C. refulgens, Neoconorbina* sp. and *R. spinulosa,* Table S1) suggestive of sedimentation under hydrodynamic and oxygenated conditions, probably adjacent to algal prairies (Jorissen, 1987; Langer, 1993; Barmawidjaja et al., 1995a).

According to the mollusk fauna, the prevalent motif of the interval between 20 and 60 m is a relatively calm mode, documented by a highly diverse epifaunal and infaunal macrofauna. The presence of holoplanktic mollusks between ca. 30–60 m documents pelagic input within a relatively distant and deep shelfal environment. Layers dominated by *Turritellina tricarinata*, *Corbula gibba* and *Ditrupa arietina*, indicate occasional sedimentary instability driven by important silting.

The upper part of the pre-unconformity interval, between ca 58 and 66.4 m, shows an increase in sand proportion and inner shelf foraminiferal assemblage, suggesting shallowing water depth (Fig. 4). The microfauna assemblage across this interval shows a drastic trend towards more abundant infralittoral species.

Specifically, both *A. beccari* and *A. parkinsoniana* (Table S1) are found also at 39.2 m, but their occurrence steadily increases from 63.6 m and 65.2 m, respectively. This pattern suggests a shallowing of the water depth below the unconformity, in line with the observations made by Jorissen, (1987).

Furthermore, a gradual sandy transition is observed between 58 and 66.4 m, and carbonate concretions developed along strata to form MDC slabs (Figs. 3, 5). These latter appear intensely bored by infralittoral lithodomes (*Lithophaga lithophaga*), nestled as well by other bivalves, such as *Hiatella arctica*, *Petricola* sp. and encrusted by *Titanoderma* sp. These slabs were obviously eroded and exposed at the seabed, then exploited by micro- and macroborers. After a sharp decrease observed in the entire microfossil foraminiferal assemblage at 65.2 m, epiphytic taxa exhibit a sudden increase, reaching up to 59% (Fig. 4) Among them, the motile epiphytic suspension feeder *E. crispum* (Langer, 1993) (Table S1) begins its increasing trend at 66 m, just below the unconformity, peaking at 66.8 m within the rhodolith horizon. The presence of this species, which is also typical in sandy environments, suggests shallowing water depth before the unconformity.

6.2. Paleoenvironmental reconstruction on the post-unconformity inner shelf interval

The firm to hard ground at the unconformity favored the rhodalgal colonization during the transgression, reworking deposits supplied from the paleo-Enza river (Figs. 3, 7). Rhodoliths form the basal lag of a thick coarse bed (R1 in Fig. 5). The small box works and pralines (Table 1) possibly identify coastal detrital bottoms under unstable edaphic conditions, with affinities with species representative of coarse sedimentary bottoms, and in correspondence of currents for L. *racemus* specimens (Pérès and Picard, 1964; Pérès, 1982; Basso, 1998). Even the other identified genera, *Lithothamnion* and *Titanoderma,* are compatible with coastal detrital bottoms, therefore suggesting the rhodolith bed formed after subaerial erosion as transgressive lag in a deepening coastal to offshore setting. Based upon literature data, the growth-rate of rhodoliths ranges between 1.08 mm/yr for tropical shallow water (Caragnano et al., 2016) down to 0.004 mm/yr for deep (>90 m) Mediterranean Sea (Bracchi et al., 2019). Considering available data on present day

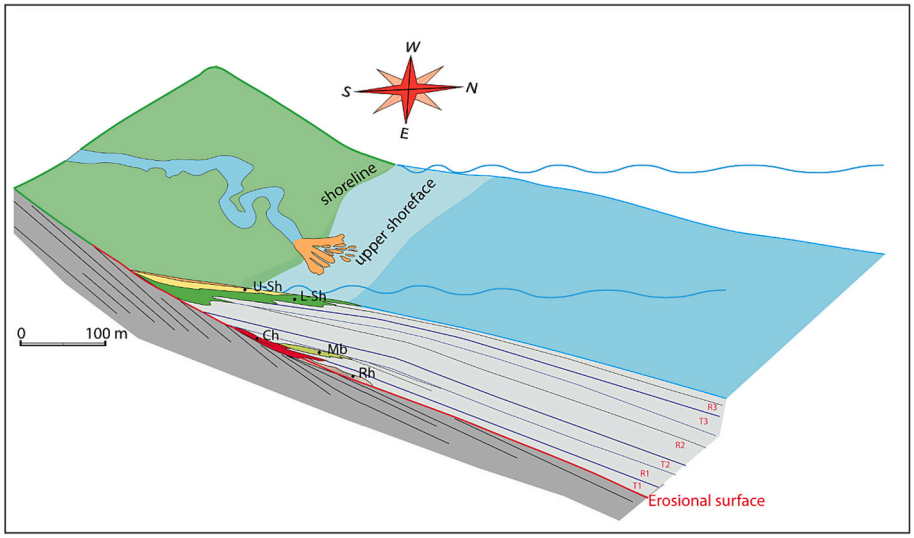

Fig. 7. Three-dimensional paleoenvironmental setting at 1.071 Ma (top of the studied Enza section). The erosional surface was generated by the co-occurring effect of tectonic uplift and sea level drop at MIS 38. The new shallow sea setting was colonized by rhodoliths (Rh) and started to receive coarse detrital supply, due to steeper and closer land drainage. Hyperpycnal subaqueous flows are common and fill channels (Ch) in the coastal to inner shelf environments. The system evolves towards mouth bar (Mb) (cycle T1/R1). A deeper prodelta deposition marks sea level rise within the shelf environments and sandy sediment had been then supplied to the inner shelf, mainly reworked by storm currents (cycle T2/R2). The last transgressive mudstone interval is followed by a thick shoreface component and coastal progradation (L-Sh Lower shoreface, U-Sh upper shoreface) (cycle T3/R3). Bold blue lines indicate the interpreted maximum flooding surfaces. (For interpretation of the references to colour in this figure legend, the reader is referred to the web version of this article.)

mesophotic rhodolith beds (Blake and Maggs, 2003; Amado-Filho et al., 2012), we can consider a medium growth-rate of 0.1–0.15 mm/yr. Based on their dimension, the rhodolith colonization likely developed in ca. 5 ka, a short time interval likely representing the local response to the sea-level rise (T1 in Fig. 7) at the transition MIS 38 to 37.

The microfauna foraminiferal assemblage across this interval exhibits significant fluctuations in the abundance of epiphytic and inner shelf species (Fig. 4). Notably, *A. beccarii*, *A. parkinsoniana*, and *E. crispum* (Table S1), which typically inhabit infralittoral environments (Morigi et al., 2005), are abundant in the bioclastic sands. This abundance may suggest that these species within the bed are reworked.

Noteworthy, at 68 m, among foraminifera, *A. mamilla*, peaks (nearly 40% of total) at the top of the first rhodolithic bed. This herbivore species, temporarily motile (Murray, 2006), may live in epifaunal microhabitat on non-vegetate sea-bottom, depending on nutritional conditions and type of substrate (Langer, 1993; Sgarrella and Moncharmont Zei, 1993; Mateu-Vicens et al., 2010). Furthermore, *A. mamilla* is presently observed in the outer shelf of the eastern Mediterranean to prefer carbonate-rich sands (Avnaim-Katav et al., 2020).

According to Van der Zwaan et al., 1999, many epiphytic species, such as *A. mamilla*, are sensitive to oxygen-limited conditions and are likely to thrive in oligotrophic environments characterized by rapid and episodic food supply (Barrasa et al., 2014). Therefore, the occurrence of this species suggests a connection with the abundant calcareous material and aligns with the deposition of labile organic matter-rich mud plume above the rhodolithic bed (Fig. 3), which serves as a resource exploited by this species.

The mudstone interval covering the rhodolithic bed was formed offshore at the stillstand of high sea-level (likely MIS 37, Fig. 6). The subsequent erosional channel at 68–70 m in the section, in turn, represents the first evidence of the approaching of the Enza fan-delta system, whose presence will characterize the facies development in the upper part of the section towards a supply dominated shelf (Swift et al., 1992). This composite coarse bed is followed by transgressive offshore mudstones (top at 76.5 m) and regressive mouth bar sandstones (Figs. 3, 7). The siliciclastic sedimentation went on with a similar shallowing upwards parasequence, starting with offshore mudstones, representing the transgressive trend, (interval between 82 and 93 m, T2 in Figs. 6, 7), further suggested by sand fraction content lower than 16% in weight in the amalgamated and bioturbated grey mudstones (Fig. 4). The latter mudstone interval is enriched in organic matter and shows an increase of the *Bulimina* group and *V. bradyana*. These mud-dwelling foraminiferal species are commonly associated with fine-grained sediments, where their abundance is primarily controlled by factors such as high food availability and low oxygen concentrations (e.g., Jorissen et al., 1992; Gupta and Machain-Castillo, 1993; Ohga and Kitazato, 1997; Bernhard and Sen Gupta, 1999; Van der Zwaan et al., 1999; Rijk et al., 2000; Mendes et al., 2004; Morigi et al., 2005). Moreover, *V. bradyana* is considered an excellent indicator of organic matter rich sediment, where periodic environmental stress conditions, such as hypoxia, occur (Jorissen, 1987, 1988; Fontanier et al., 2002). We can conclude that the micro and macrofossil assemblages are overall consistent with a prodeltaic setting, episodically subjected to noticeable silting. It likely records the maximum deepening in the post-unconformity succession (Fig. 7).

This transgressive interval ends with the regressive sandy-muddy storm wave base deposits (93–118 m) (Figs. 3, 4). Storm-layers (tempestites) are supplied by infralittoral sources, from sandy and muddy inner shelfal environments. Noteworthy, the base of some storm layer is marked by disarticulated and at times blackened bivalves, including *Arctica islandica* and the foraminiferal assemblage (Table S1) shows a general increase *of A. beccarii*, *A. parkinsoniana* and *A. tepida*, corresponding to the cluster S9 F3 of Barbieri et al. (2019), indicating inner shelf (i.e., water depth) with mixed substrates (mud-sand) and a variable organic matter amount.

Then from 96 m onward, the foraminifera assemblage from the muddy intervals shows fluctuations of *A. beccari*, along with increasing *A. tepida* from 0% to 5%, indicate shallow sea conditions. Furthermore, *A. tepida* is a stress tolerant species presently found in estuaries and lagoons of various regions, including southern California, Brazil, Venice lagoon, the UK, Australia, and Indonesia (e.g. Raynusha et al., 2020; Laut et al., 2021; Schweizer et al., 2022) This species can thrive in a wide range of salinity and temperature conditions in nearshore environments, such as shallow marine, lagoonal, and deltaic zones. According to Jorissen (1988), the current distribution of *A. tepida* is closely related to the Po runoff system. Its abundance in the studied section suggests salinity variations due to the proximity of the delta system. (Fig. 7). Finally, In the upper part of the studied section, other significant fluctuations in foraminiferal microfossils are recorded and can be interpreted as follows:

at 102 m, the dominance of *P. granosum* (43%) along with the occurrence of *A. perlucida* (25%) suggests a high sedimentation infralittoral setting with muddy substrates characterized by high organic matter content (Jorissen, 1987; Barmawidjaja et al., 1995; Jorissen et al., 2018), but not oxygen depleted; at 108 m, the *Textularia* group occurs in greater abundance (maximum 11%), along with the *Quinqueloculina* group (7%). These grazing epiphytic taxa (Langer, 1993) suggest a wave-dominated sandy shoreface with low organic matter input (Jorissen et al., 1992); at 116 m, *E. decipiens* (34%) and *A. perlucida* (28%) dominate the assemblage, and *A. parkinsoniana* and *A. tepida* also occur, though in lower frequencies. These species tolerate relatively high organic matter concentrations and prefer muddy substrates (cluster S9F3 of Barbieri et al. (2019). The observed peak of *E. decipiens*, according to Barbieri et al. (2019), suggests a moderate riverine input.

The last studied cycle from 118 to 136 m, shows a transgressive 7 m thick mudstone interval (T3 in Fig. 7) followed by a thick shoreface component, with relevant traces of subaerial exposures (Pizzati et al., 2018).

This reconstruction therefore evidences the existence of T/R cycles that were more and more shallow upward. This occurred when the coastline was already oriented NW-SE, following the main structural direction of the mountain front (Fig. 7). Our reconstruction slightly predates the one reported by Ghielmi et al. (2013) for the Middle Pleistocene PS2 sequence where, eastward of the study section, a N-S-oriented shelf edge has been dated at 900 ka.

6.3. Tectonic forcing in the Enza section and the growth of the mountain front

The Enza section shows very clear growing stratigraphy, dominated by divergent pattern interrupted by a prominent angular unconformity (Gunderson et al., 2014). This unconformity represents a time gap estimated around 140 ka, due to missing sedimentation and erosion of the underlying mudstones, till the more resistant carbonate concretions. The deformation progressively affected younger intervals, and the Enza succession is tilted up to its top (top Middle Pleistocene). Previous papers dealt with the tectonic setting of the Apennine mountain front in the area, and the interested readers are referred to the maps and cross sections in Ponza, (2010), Gunderson et al. (2014) and Oppo et al. (2013, 2015). A similar growing stratigraphy on the Stirone river, located at the same mountain front some 40 km to the west, has been modeled by Gunderson et al. (2013). These authors explained the progressive tilting of the mountain front with a combined frontal limb folding of two blind thrust ramps located at different depths. The most superficial one has a tip propagating from 5 to 3 km below the surface, the deeper one propagating from 21 to 17 km (see Fig. 8). Whereas the superficial one was active from 3 to 1.8 Ma, decelerating to around 1 Ma, when it ended its activity, the deeper one started at around 1.8 and possibly increased its activity after 1 Ma (Gunderson et al., 2013).

In Table 2, we adopted the tilt rate of the Enza succession as an indicator of the activity of two thrust structures at different depth of the mountain front: the superficial Quattro Castella thrust-related anticline

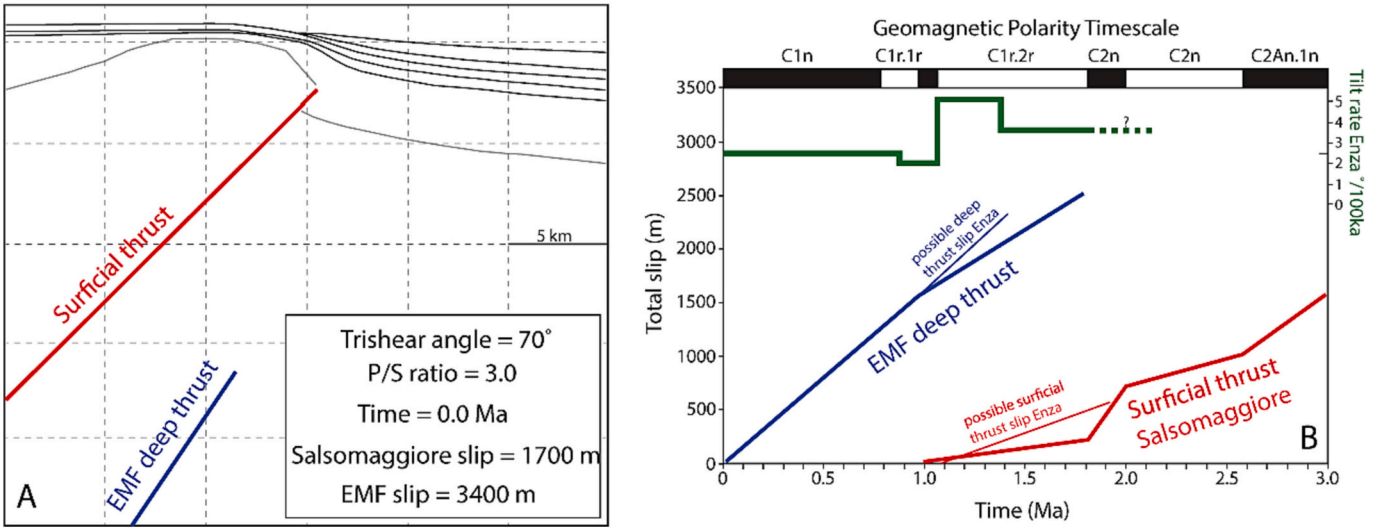

Fig. 8. A) Inversion of the tilted beds at the mountain front of the Apennines at Salsomaggiore,

Table 2
Reconstruction of the tilt rates recorded by the Enza section. Age attribution of time intervals derives from the chronology discussed in this paper. Bed dips are from Gunderson et al. (2014) and Pizzati et al. (2018) and show the tilt rate up to present.

Enza log interval	Time duration	Dip variation After Gunderson et al., 2014 and Pizzati et al., 2018	Tilt rate
Pre-unconformity	1.733–1.38 Ma = 353 ka	54° - 42° = 12°	3.6° /100 ka
Angular unconformity	1.385–1.245 Ma = 140 ka	42°- 35° = 7°	5.1° /100 ka
Post unconformity	1.248–1.071 Ma = 177 ka	35°- 26° = 9°	5.1°/ 100 ka
Sabbie Gialle	1.071–0.87 Ma = 201 ka	26°- 22 = 4°	2° /100 ka
Synthem AEI	0.87–0.4 Ma = 470 ka	22°- 10° = 12°	2.5° /100 ka
Synthem AES	0.4–0.0 Ma = 400 ka	10°- 0° = 10°	2.5° /100 ka

(Fig. 2) and the deeper thrust, highlighted by some studies as the responsible of the recent deformation of the mountain front of the Emilia, from Bologna (Picotti and Pazzaglia, 2008) to Salsomaggiore to the west (Emilia Mountain Front EMF of (Gunderson et al., 2013) (Fig. 8).

From the data in Table 2, we interpret the 3.6°/100 ka tilt rate of the pre-unconformity interval as related to the activity of the Quattro Castella anticline (Fig. 2). The tilt rate increased up to 5.1°/100 ka in the interval 1.38 to 1.071 Ma, and it is very likely providing the pre-conditions for the angular unconformity (Fig. 8).

40 km to the northwest of the Enza, according to a trishear geometry of two thrust structures, a surficial (Salsomaggiore thrust) and a deeper one (EMF), best fit model of Gunderson et al. (2013). B) Slip histories of the two structures, with proposed deviation from the Gunderson et al. (2013) model in the case of the Enza. Modified after Gunderson et al. (2013). In green, the tilt rate recorded at the Enza, showing a maximum during the joint activity of the two thrusts.

It can be interpreted, following Gunderson et al. (2013), as due to the combined activity of the two thrust structures. The deeper thrust, in fact, seems responsible for the increase of 2–2.5°/100 ka tilt rate, almost constantly recorded in the stratigraphy of the last 1.071 Ma, also after the cessation of the Quattro Castella thrust, whose tilt rate was slightly higher in the order of 3–3.6°/100 ka. Gunderson et al. (2013) modeled for the Stirone section a time interval between 1.8 and 1 Ma when the two structures were both active, the most surficial one fading out till its stop. In the case of the Enza, we observe a similar behavior, and we can constrain the overlap between the two thrust structures to a shorter time interval between 1.38 and 1.071 Ma. After that time, due to the deactivation of the thrust creating the Quattro Castella anticline, only the deep EMF structure will keep its activity, folding the Pleistocene strata with a 2–2.5°/ ka (Fig. 8).

6.4. *Eustatic forcing in the Enza section at the onset of the Mid-Pleistocene Transition*

During the Mid-Pleistocene Transition (MPT 1250–800 ka), Earth's orbitally paced ice age cycles intensified, lengthened from~40 to~100 ka, and became distinctly asymmetrical (e.g., (Chalk et al., 2017). The intensification of the glacial/interglacial cycles at the onset of the MPT is associated to wider oscillations of the eustatic sea-level (Miller et al., 2005). The pre-unconformity interval at the Enza section (1730 to 1385 ka), with its continuous deposition, suggests any eustatic oscillations should have been less ample than the available bathymetry in this outer shelf. As the $\delta^{18}O$ based sea-level reconstruction of Miller et al. (2005) suggests peak drawdowns in the order of 50 to 70 m maximum, we infer that the outer shelf paleobathymetry at the Enza section was constantly deeper than 50 to 70 m in the pre-unconformity succession. As an alternative, we could infer that this muddy outer shelf of the pre-unconformity Enza interval was indeed affected by sea-level minima, which, however, were not associated with dramatic facies changes for their short duration or not sufficient amplitude. Our record, however, shows that in the topmost part of the section, before the unconformity and where the stable isotope record indicates the occurrence of three oscillations correlated to MIS 49/48, 47/46 and 45/44, inner shelf foraminifera increase in abundance. This fact can be interpreted either as a sign of increasing amplitude of the eustatic oscillations, or as first evidence of a progressive shallowing of the bathymetry, or both. Miller et al. (2005) reconstructed a − 69 m sea-level drawdown for the MIS 46 (Fig. 6), at around 1420 ka. Due to the estimated time gap at the unconformity, we cannot discuss the potential effects of the drawdowns related to MIS 44 to 40 (1380 to 1255 ka). For these reasons, in a context of increasing tilting of the mountain front, we suggest that the ultimate responsible for the angular unconformity was the enhanced sea level drawdowns at the onset of the MPT.

The post-unconformity succession can be interpreted as a stack of cyclothemes, not always well expressed, associated to eustatic oscillations of high frequency and amplitude. These cyclothemes, interpreted as 5th order cycles, are arranged into lower frequency T/R cycles, likely

corresponding to 4th order parasequences (Fig. 6). The rhodolith beds corresponds to a very peculiar and laterally discontinuous transgressive unit, the overlying pelitic interval represents the offshore facies, grading to sand dominated fluvial mouth bar during depositional regressions at the sea-level highstand (see Pillans et al., 1998). Firm-ground are locally observed on top of the sandy intervals, like the *Ditrupa* bed at 82 m, suggesting the subsequent marine transgression was reworking the underlying (ravinement) surface, likely emerged during the sea-level lowstand (Fig. 7). Evidence of subaerial exposure characterizes the upper cyclothemes, with carbonate concretions in the 128 to 142 m interval associated to the development of soils, removed by the subsequent transgression (Pizzati et al., 2018). Interestingly, the duration of the first T/R cycle after the recovery of the sedimentation is around 40 ka, whereas the subsequent ones have longer duration, 80 ka. This sharp increase in frequency is likely heralding the effects of the MPT.

The latter had a strong impact on the Enza section. The sharp doubling of the sedimentation rate across the unconformity is significant of the overall increase of the sediment supply from the surrounding mountain belt and the enhanced progradation of the clastic systems, possibly associated with changing biomes and connectivity on the hillslopes. In this overall shallowing trend of the succession, the intensified eustatic drawdown of the MIS 38 (1255 ka) impacted the shelf, eroding and leaving the area in subaerial conditions for several thousands of years. The post-unconformity unit was formed by 5th order cycles, very likely in pace with the eustatic signal and arranged into T/R parasequences. In this respect, thanks to the increased sedimentation rates, the ongoing tectonic deformation did not exert any control on the facies architecture of this part of the sedimentary record.

7. Conclusions

The sedimentological, paleontological and the $\delta^{18}O$ record of the Enza section, by now a reference section for the Pleistocene in the Mediterranean, has been studied into details to unravel the role of tectonics at the mountain front of the Northern Apennines and of climate at the onset of the MPT.

Our results allow defining the paleoenvironment of the pre-unconformity outer shelf, an oxygenated bottom dominated by diffusive distribution of sediment. The upward increase of the percentage of sand and inner shelf fossil species in the uppermost 8–10 m (from around 57 to 66.4 m) documents the shallowing of the bathymetry, in a context of an average sedimentation rate of 20 cm/ka, clearly sufficient to outpace the local subsidence. The new $\delta^{18}O$ data allowed us correlating the last 14 m underneath the unconformity to the MIS 49 to 45, improving our understanding of the time duration of the sedimentary gap, now bracketed between around 1380 and 1245 ka. The sea-level drawdown of the MIS 38 peaking at 1255 ka (Miller et al., 2005; Gibbard and Head, 2020) is the most relevant drawdown since the beginning of the Pleistocene (−92 m, Miller et al., 2005), to be considered the onset of the MPT (e.g., Clark et al., 2006; Chalk et al., 2017; Herbert, 2023). This is the best candidate for the event responsible for the unconformity.

The post MIS 38 transgression at the Enza is expressed by the rhodolithic bed, a peculiar feature that took several thousands of years to form, according to the paleoecology of the algae. Overall, the post-unconformity studied succession in the Enza was formed during increasing amplitude transgressive/regressive cycles and sedimentation rates. The paleo-Enza river was influencing the facies since the first rhodolithic deposits, with incised channel and deltaic contributions to the shore deposits. In this context, the paleoenvironmental data confirm the prodeltaic character of the mudstones of the first T/R cycles, and the mouth bar facies of their topping sands. The exposure of the top of the cyclothems becomes more relevant in the upper part of the section, as confirmed by the increasing abundance of carbonate concretions of meteoric origin.

The studied section at the Enza river shed new light on the evolution of the mountain front of the Northern Apennines. The tilting rate variations reconstructed for the Enza section document the superimposed activity of the frontal limb of two structures: the Quattro Castella ramp anticline and a deeper, mid-crustal thrust responsible of the Northern Apennines mountain front (Picotti and Pazzaglia, 2008; EMF of Gunderson et al., 2013). In the case of the Enza, the Quattro Castella ramp anticline ceased its activity at around 1 Ma, whereas, starting at around 1.3 Ma, the lower but steady tilt rate occurring afterwards can be related to the EMF deeper thrust, still active, as documented by Late Pleistocene and Holocene deformed features (Picotti and Pazzaglia, 2008; Ponza, 2010). The co-occurrence of two thrusts, a surficial and a deeper one, can explain the increased tilting rate between 1.3 and 1 Ma, as well as the doubled subsidence rate during this same period.

Based on our reconstruction, the paleogeography in the Enza section preludes the major reshaping of the western sector of northern Apennine foredeep, expressed by a major re-orientation of the coastline in a North-South direction. The stratigraphic architecture of the Enza section is a dramatic expression of the changing pace of Earth's climate at the onset of the MPT. On one hand, the intensification of the erosion on land, likely driven by the erosional impact of the seasonal intensification, brought about the doubling of the sedimentation rate across the unconformity, notwithstanding the interruptions of the sedimentation due to emersions in the second part of the section. On the other hand, the transition from a continuous outer shelf sedimentation to a cyclothemic deposition, likely controlled by the eustatic oscillations, suggests a sharp passage towards increasing amplitude of the T/R cycles. These fingerprints of the MPT occur not only of the Enza section in the Northern Apennines, but also in other Mediterranean settings (e.g., Crotone basin, Massari et al., 1999) and other basins (South China Sea, Liu et al., 2022).

CRediT authorship contribution statement

Rossella Capozzi: Conceptualization, Investigation, Visualization, Writing – original draft, Writing – review & editing. **Vincenzo Picotti:** Conceptualization, Investigation, Visualization, Writing – original draft, Writing – review & editing. **Valentina Alice Bracchi:** Investigation, Writing – review & editing. **Francesca Caridi:** Investigation, Writing – review & editing. **Anna Sabbatini:** Investigation, Writing – review & editing. **Marco Taviani:** Investigation, Writing – review & editing. **Stefano Bernasconi:** Investigation, Writing – review & editing. **Alessandra Negri:** Conceptualization, Investigation, Visualization, Writing – original draft, Writing – review & editing.

Declaration of competing interest

The authors declare that they have no known competing financial interests or personal relationships that could have appeared to influence the work reported in this paper.

Data availability

Table S1, Table S2

Acknowledgments

The research benefited of the MIUR PRIN 2009 prot. 2009WCYS5P funds to RC, AN and MT. We are deeply indebted to Kellen Gunderson and Frank Pazzaglia for sharing samples and fieldwork data. Simone Cau, Paolo Montagna and Daniele Scarponi are warmly thanked for fruitful discussion during the fieldwork. We are grateful to H. Dowsett and the two anonymous reviewers for their particularly useful comments that helped us to improve the manuscript.

This is ISMAR-CNR, Bologna, scientific contribution n. 2079.

Appendix A. Supplementary data

Supplementary data to this article can be found online at https://doi.org/10.1016/j.palaeo.2024.112087.

References

Agip, S., 1982. Foraminiferi Padani (Terziario e Quaternario): Atlante iconografico e distribuzione stratigrafica. Milano.

Allin, J.R., Hunt, J.E., Clare, M.A., Talling, P.J., 2017. Eustatic sea-level controls on the flushing of a shelf-incising submarine canyon. Geol. Soc. Am. Bull. 130 (1/2), 223.

Amado-Filho, G.M., Pereira-Filho, G.H., Bahia, R.G., Abrantes, D.P., Veras, P.C., Matheus, Z., 2012. Occurrence and distribution of rhodolith beds on the Fernando de Noronha Archipelago of Brazil. Aquat. Bot. 101, 41–45.

Amorosi, A., Colalongo, M.L., Fusco, F., Pasini, G., Fiorini, F., 1999. Glacio-eustatic control of continental–shallow marine cyclicity from late Quaternary deposits of the southeastern Po Plain, northern Italy. Quat. Res. 52 (1), 1–13.

Avnaim-Katav, S., Almogi-Labin, A., Kanari, M., Herut, B., 2020. Living benthic foraminifera of southeastern Mediterranean ultra-oligotrophic shelf habitats: Implications for ecological studies. Estuar. Coast. Shelf Sci. 234, 106633.

Barbieri, G., Rossi, V., Vaiani, S.C., Horton, B.P., 2019. Benthic ostracoda and foraminifera from the North Adriatic Sea (Italy, Mediterranean Sea): A proxy for the depositional characterisation of river-influenced shelves. Mar. Micropaleontol. 153, 101772 https://doi.org/10.1016/j.marmicro.2019.101772.

Barmawidjaja, D.M., Van der Zwaan, G.J., Jorissen, F.J., Puskaric, S., 1995a. 150 years of eutrophication in the northern Adriatic Sea: evidence from a benthic foraminiferal record. Mar. Geol. 122 (4), 367–384.

Barmawidjaja, D.M., Van der Zwaan, G.J., Jorissen, F.J., Puskaric, S., 1995b. 150 years of eutrophication in the northern Adriatic Sea: evidence from a benthic foraminiferal record. Mar. Geol. 122 (4), 367–384.

Barrasa, C., Jorissena, F.J., Labruneb, C., Andrald, B., Boisserye, P., 2014. Live benthic foraminiferal faunas from the French Mediterranean Coast: towards a new biotic index of environmental quality. Ecol. Indic. 36, 719–743.

Basso, D., 1998. Deep rhodolith distribution in the Pontian Islands, Italy: a model for the paleoecology of a temperate sea. Palaeogeogr. Palaeoclimatol. Palaeoecol. 137 (1–2), 173–187.

Berends, C.J., Köhler, P., Lourens, L.J., Van de Wal, R.S.W., 2021. On the Cause of the Mid-Pleistocene Transition. Wiley Online Library.

Berger, A., Loutre, M.F., 2000. CO2 and astronomical forcing of the late quaternary. In: The Solar Cycle and Terrestrial Climate, Solar and Space Weather, 463, p. 155.

Bernasconi, S.M., Müller, I.A., Bergmann, K.D., Breitenbach, S.F., Fernandez, A., Hodell, D.A., Jaggi, M., Meckler, A.N., Millan, I., Ziegler, M., 2018. Reducing uncertainties in carbonate clumped isotope analysis through consistent carbonate-based standardization. Geochem. Geophys. Geosyst. 19 (9), 2895–2914.

Bernhard, J.M., Sen Gupta, B.K., 1999. Foraminifera of oxygen-depleted environments. In: Modern Foraminifera. Springer, pp. 201–216.

Bernhard, J.M., Tsuchiya, M., Nomaki, H., 2018. Ultrastructural observations on prokaryotic associates of benthic foraminifera: food, mutualistic symbionts, or parasites? Mar. Micropaleontol. 138, 33–45. https://www.sciencedirect.com/science/article/pii/S0377839817300567.

Blake, C., Maggs, C.A., 2003. Comparative growth rates and internal banding periodicity of maerl species (Corallinales, Rhodophyta) from northern Europe. Phycologia 42 (6), 606–612.

Blumenberg, M., Walliser, E.-O., Taviani, M., Seifert, R., Reitner, J., 2015. Authigenic carbonate formation and its impact on the biomarker inventory at hydrocarbon seeps–a case study from the Holocene Black Sea and the Plio-Pleistocene Northern Apennines (Italy). Mar. Pet. Geol. 66, 532–541.

Boccaletti, M., Coli, M., Eva, C., Ferrari, G., Giglia, G., Lazzarotto, A., Merlanti, F., Nicolich, R., Papani, G., Postpischl, D., 1985. Considerations on the seismotectonics of the Northern Apennines. Tectonophysics 117 (1–2), 7–38.

Borghi, E., 2021. Gli schizasteridi (Echinoidea) del Plio-Pleistocene dell'Emilia. In: Notiziario della Società Reggiana di Scienze Naturali, 2020, pp. 20–38.

Bosence, D.W., 1983. Description and classification of rhodoliths (rhodoids, rhodolites). Coat. Grains 217–224.

Bracchi, V.A., Angeletti, L., Marchese, F., Taviani, M., Cardone, F., Hajdas, I., Grande, V., Prampolini, M., Caragnano, A., Corselli, C., 2019. A resilient deep-water rhodolith bed off the Egadi Archipelago (Mediterranean Sea) and its actuopaleontological significance. Alp. Mediterr. Quat. 32 (2), 131–150.

Braga, J.C., 2003. Application of botanical taxonomy to fossil coralline algae (Corallinales, Rhodophyta). Acta Micropaleontol. Sin. 20, 47.

Breitenbach, S.F., Bernasconi, S.M., 2011. Carbon and oxygen isotope analysis of small carbonate samples (20 to 100 μg) with a GasBench II preparation device. Rapid Commun. Mass Spectrom. 25 (13), 1910–1914.

Bressan, G., 2003. Corallinales del Mar Mediterraneo: Guida alla determinazione.

Brocchi, G.B., 1814. Conchiologia fossile subapennina con osservazioni geologiche sugli Apennini e sul suolo adiacente di G. Brocchi... Con sedici tavole in rame. Tomo primo [–secondo]: 1. Stamperia reale.

Calderoni, G., Di Giovambattista, R., Burrato, P., Ventura, G., 2009. A seismic sequence from Northern Apennines (Italy) provides new insight on the role of fluids in the active tectonics of accretionary wedges. Earth Planet. Sci. Lett. 281 (1–2), 99–109.

Capozzi, R., Negri, A., Reitner, J., Taviani, M., 2015. Carbonate conduits linked to hydrocarbon-enriched fluid escape. Mar. Pet. Geol. 66, 497–500.

Capozzi, R., Oppo, D., Taviani, M., 2017. Cold seepages: an economic tool for hydrocarbon appraisal. AAPG Bull. 101 (4), 617–623.

Caragnano, A., Basso, D., Rodondi, G., 2016. Growth rates and ecology of coralline rhodoliths from the Ras Ghamila back reef lagoon, Red Sea. Mar. Ecol. 37 (4), 713–726.

Chalk, T.B., Hain, M.P., Foster, G.L., Rohling, E.J., Sexton, P.F., Badger, M., 2017. Causes of ice-age intensification across the Mid-Pleistocene Transition. Transition 114, 13114–13119 (s.d.).

Clark, P.U., Archer, D., Pollard, D., Blum, J.D., Rial, J.A., Brovkin, V., Mix, A.C., Pisias, N. G., Roy, M., 2006. The middle Pleistocene transition: characteristics, mechanisms, and implications for long-term changes in atmospheric pCO2. Quat. Sci. Rev. 25 (23–24), 3150–3184.

Ellerton, D., Rittenour, T.M., Shulmeister, J., Roberts, A.P., Miot da Silva, G., Gontz, A., Hesp, P.A., Moss, P., Patton, N., Santini, T., 2022. Fraser Island (K'gari) and initiation of the Great Barrier Reef linked by Middle Pleistocene Sea-level change. Nat. Geosci. 15 (12), 1017–1026.

Fontanier, C., Jorissen, F.J., Licari, L., Alexandre, A., Anschutz, P., Carbonel, P., 2002. Live benthic foraminiferal faunas from the Bay of Biscay: Faunal density, composition, and microhabitats. Deep-Sea Res. I Oceanogr. Res. Pap. 49 (4), 751–785. https://doi.org/10.1016/S0967-0637(01)00078-4.

Fontanier, C., Jorissen, F.J., Lansard, B., Mouret, A., Buscail, R., Schmidt, S., Kerhervé, P., Buron, F., Zaragosi, S., Hunault, G., 2008. Live foraminifera from the open slope between Grand Rhône and Petit Rhône canyons (Gulf of Lions, NW Mediterranean). Deep-Sea Res. I Oceanogr. Res. Pap. 55 (11), 1532–1553. https://www.sciencedirect.com/science/article/pii/S0967063708001477.

Fornaciari, E., Rio, D., Ghibaudo, G., Massari, F., Iaccarino, S., 1997. Calcareous plankton biostratigraphy of the Serravallian (Middle Miocene) stratotype section (Piedmont Tertiary basin, NW Italy). Mem. Sci. Geol. 49, 127–144.

Ghielmi, M., Minervini, M., Nini, C., Rogledi, S., Rossi, M., 2013. Late Miocene–Middle Pleistocene sequences in the Po Plain–Northern Adriatic Sea (Italy): the stratigraphic record of modification phases affecting a complex foreland basin. Mar. Pet. Geol. 42, 50–81.

Gibbard, P.L., Head, M.J., 2020. The quaternary period. In: Geologic Time Scale 2020. Elsevier, pp. 1217–1255.

Goineau, A., Fontanier, C., Jorissen, F.J., Lansard, B., Buscail, R., Mouret, A., Kerhervé, P., Zaragosi, S., Ernoult, E., Artéro, C., 2011. Live (stained) benthic foraminifera from the Rhône prodelta (Gulf of Lion, NW Mediterranean): Environmental controls on a river-dominated shelf. J. Sea Res. 65 (1), 58–75. https://www.sciencedirect.com/science/article/pii/S1385110110001012.

Guiry, M.D., Guiry, G.M., 2020. AlgaeBase. World-wide electronic publication, National University of Ireland, Galway, Ireland.

Gunderson, K.L., Anastasio, D.J., Pazzaglia, F.J., Picotti, V., 2013. Fault slip rate variability on 104–105 yr timescales for the Salsomaggiore blind thrust fault, Northern Apennines, Italy. Tectonophysics 608, 356–365.

Gunderson, K.L., Pazzaglia, F.J., Picotti, V., Anastasio, D.A., Kodama, K.P., Rittenour, T., Frankel, K.F., Ponza, A., Berti, C., Negri, A., 2014. Unraveling tectonic and climatic controls on synorogenic growth strata (Northern Apennines, Italy). Bulletin 126 (3–4), 532–552.

Gupta, B.K.S., Machain-Castillo, M.L., 1993. Benthic foraminifera in oxygen-poor habitats. Mar. Micropaleontol. 20 (3–4), 183–201.

Herbert, T.D., 2023. The Mid-Pleistocene climate transition. Annu. Rev. Earth Planet. Sci. 51, 389–418.

Hönisch, B., Hemming, N.G., Archer, D., Siddall, M., McManus, J.F., 2009. Atmospheric carbon dioxide concentration across the mid-Pleistocene transition. Science 324 (5934), 1551–1554.

Hrabovskỳ, J., Basso, D., Doláková, N., 2016. Diagnostic characters in fossil coralline algae (Corallinophycidae: Rhodophyta) from the Miocene of southern Moravia (Carpathian Foredeep, Czech Republic). J. Syst. Palaeontol. 14 (6), 499–525.

Iaccarino, S., Monegatti, P., 1996. La successione pleistocenica del Torrente Enza: XIII Convegno SocietaPaleontologica Italiana. Excursion Guidebook. Universitadi Parma, Parma, pp. 63–67.

Irvine, L.M., Chamberlain, Y.M., 1994. Volume 1 Rhodophyta Part 2B Corallinales, Hildenbrandiales. Natural History Museum, London, pp. 1–30.

Jelby, M.E., Grundvåg, S.-A., Helland-Hansen, W., Olaussen, S., Stemmerik, L., 2020. Tempestite facies variability and storm-depositional processes across a wide ramp: towards a polygenetic model for hummocky cross-stratification. Sedimentology 67 (2), 742–781.

Jorissen, F.J., 1987. The distribution of benthic foraminifera in the Adriatic Sea. Mar. Micropaleontol. 12, 21–48.

Jorissen, F.J., 1988. Benthic foraminifera from the Adriatic Sea: principles of phenotypic variation. Utrecht Micropaleontol. Bull. 37. https://dspace.library.uu.nl/handle/1874/205896.

Jorissen, F.J., Barmawidjaja, D.M., Puskaric, S., Van der Zwaan, G.J., 1992. Vertical distribution of benthic foraminifera in the northern Adriatic Sea: the relation with the organic flux. Mar. Micropaleontol. 19 (1–2), 131–146.

Jorissen, F., Nardelli, M.P., Almogi-Labin, A., Barras, C., Bergamin, L., Bicchi, E., El Kateb, A., Ferraro, L., McGann, M., Morigi, C., Romano, E., Sabbatini, A., Schweizer, M., Spezzaferri, S., 2018. Developing Foram-AMBI for biomonitoring in the Mediterranean: species assignments to ecological categories. Mar. Micropaleontol. 140, 33–45. https://doi.org/10.1016/j.marmicro.2017.12.006.

Langer, M.R., 1993. Epiphytic foraminifera. Mar. Micropaleontol. 20 (3–4), 235–265.

Laut, L., da Matta, G., Camara, G., Belart, P., Clemente, I., Ballalai, J., Volino, E., da Couto, E.C.G., 2021. Living and dead foraminifera assemblages as environmental indicators in the Almada River Estuary, Ilhéus, northeastern Brazil. J. S. Am. Earth Sci. 105, 102883. https://www.sciencedirect.com/science/article/pii/S0895981120304260.

Lisiecki, L.E., Raymo, M.E., 2005. A Pliocene-Pleistocene stack of 57 globally distributed benthic δ18O records. Paleoceanography 20 (1).

Liu, X., Zhang, M., Li, A., Dong, J., Zhang, K., Gu, Y., Chang, X., Zhuang, G., Li, Q., Wang, H., 2022. Sedimentary pyrites and C/S ratios of mud sediments on the East China Sea inner shelf indicate late Pleistocene-Holocene environmental evolution. Mar. Geol. 450, 106854.

Loeblich Jr., A., Tappan, H., 1987. Foraminiferal Genera and their classification: Van Reinhold Company. N. Y. 2.

Malatesta, A., Zarlenga, F., 1988. Evidence of Middle Pleistocene marine transgressions along the Mediterranean coast. Palaeogeogr. Palaeoclimatol. Palaeoecol. 68 (2–4), 311–315.

Manda, S., Titelboim, D., Ashckenazi-Polivoda, S., Almogi-Labin, A., Herut, B., Abramovich, S., 2020. Epiphytic benthic foraminiferal preferences for macroalgal habitats: implications for coastal warming. Mar. Environ. Res. 161, 105084. https://www.sciencedirect.com/science/article/pii/S014111362030547X.

Martinetto, E., Monegato, G., Irace, A., Vaiani, S.C., Vassio, E., 2015. Pliocene and Early Pleistocene carpological records of terrestrial plants from the southern border of the Po Plain (northern Italy). Rev. Palaeobot. Palynol. 218, 148–166.

Massari, F., Sgavetti, M., Rio, D., D'alessandro, A., Prosser, G., 1999. Composite sedimentary record of falling stages of Pleistocene glacio-eustatic cycles in a shelf setting (Crotone basin, South Italy). Sediment. Geol. 127 (1–2), 85–110.

Mateu-Vicens, G., Box, A., Deudero, S., Rodríguez, B., 2010. Comparative analysis of epiphytic foraminifera in sediments colonized by seagrass Posidonia oceanica and invasive macroalgae Caulerpa spp. J. Foram. Res. 40 (2), 134–147.

Mendes, I., Gonzaleza, R., Dias, J.M.A., Lobo, F., Martins, V., 2004. Factors influencing recent benthic foraminifera distribution on the Guadiana shelf (Southwestern Iberia) $. Mar. Micropaleontol. 51, 171–192.

Miller, K.G., Kominz, M.A., Browning, J.V., Wright, J.D., Mountain, G.S., Katz, M.E., Sugarman, P.J., Cramer, B.S., Christie-Blick, N., Pekar, S.F., 2005. The Phanerozoic record of global sea-level change. science 310 (5752), 1293–1298.

Mojtahid, M., Jorissen, F., Lansard, B., Fontanier, C., Bombled, B., Rabouille, C., 2009. Spatial distribution of live benthic foraminifera in the Rhône prodelta: Faunal response to a continental–marine organic matter gradient. Mar. Micropaleontol. 70 (3–4), 177–200. https://www.sciencedirect.com/science/article/pii/S0377839808001473.

Mojtahid, M., Zubkov, M.V., Hartmann, M., Gooday, A.J., 2011. Grazing of intertidal benthic foraminifera on bacteria: assessment using pulse-chase radiotracing. J. Exp. Mar. Biol. Ecol. 399 (1), 25–34. https://doi.org/10.1016/j.jembe.2011.01.011.

Molli, G., 2008. Northern Apennine–Corsica orogenic system: an updated overview. Geol. Soc. Lond. Spec. Publ. 298 (1), 413–442.

Morigi, C., Jorissen, F.J., Fraticelli, S., Horton, B.P., Principi, M., Sabbatini, A., Capotondi, L., Curzi, P.V., Negri, A., 2005. Benthic foraminiferal evidence for the formation of the Holocene mud-belt and bathymetrical evolution in the Central Adriatic Sea. Mar. Micropaleontol. 57 (1–2), 25–49.

Murray, J.W., 2006. Ecology and Applications of Benthic Foraminifera. Cambridge university press.

Ohga, T., Kitazato, H., 1997. Seasonal changes in bathyal foraminiferal populations in response to the flux of organic matter (Sagami Bay, Japan). Terra Nova 9 (1), 33–37.

Oppo, D., Capozzi, R., Picotti, V., 2013. A new model of the petroleum system in the Northern Apennines, Italy. Mar. Pet. Geol. 48, 57e76.

Oppo, D., Capozzi, R., Picotti, V., Ponza, A., 2015. A genetic model of hydrocarbon-derived carbonate chimneys in shelfal fine-grained sediments: the Enza River field, Northern Apennines (Italy). Mar. Pet. Geol. 66, 555–565.

Pérès, J.M., 1982. Major Benthic Assemblages.

Pérès, J.-M., Picard, J., 1964. Nouveau manuel de bionomie benthique de la mer Méditerranée. Station Marine d'Endoume.

Pezzolesi, L., Peña, V., Le Gall, L., Gabrielson, P.W., Kaleb, S., Hughey, J.R., Rodondi, G., Hernandez-Kantun, J.J., Falace, A., Basso, D., 2019. Mediterranean Lithophyllum stictiforme (Corallinales, Rhodophyta) is a genetically diverse species complex: implications for species circumscription, biogeography and conservation of coralligenous habitats. J. Phycol. 55 (2), 473–492.

Picotti, V., Pazzaglia, F.J., 2008. A new active tectonic model for the construction of the Northern Apennines mountain front near Bologna (Italy). J. Geophys. Res. Solid Earth 113 (B8).

Pillans, B., Chappell, J., Naish, T.R., 1998. A review of the Milankovitch climatic beat: Template for Plio Pleistocene Sea-level changes and sequence stratigraphy. Sediment. Geol. 122 (1), 5–21.

Pizzati, M., Balsamo, F., Storti, F., Mozafari, M., Iacumin, P., Tinterri, R., Swennen, R., 2018. From axial parallel to orthogonal groundwater flow during fold amplification: insights from carbonate concretion development during the growth of the Quattro Castella Anticline, Northern Apennines, Italy. J. Geol. Soc. 175 (5), 806–819.

Ponza, A., 2010. Tectonic Geomorphology and Active Strain of the Northern Apennines Mountain Front.

Ponziani, F., De Franco, R., Minelli, G., Biella, G., Federico, C., Pialli, G., 1995. Crustal shortening and duplication of the Moho in the Northern Apennines: a view from seismic refraction data. Tectonophysics 252 (1–4), 391–418.

Raffi, I., Backman, J., Fornaciari, E., Pälike, H., Rio, D., Lourens, L., Hilgen, F., 2006. A review of calcareous nannofossil astrobiochronology encompassing the past 25 million years. Quat. Sci. Rev. 25 (23–24), 3113–3137.

Raynusha, C., Rozaimi, M., Omar, R., Faiz, N.N., Hesan, N.M., Hanis, S.N., Abdullah, S. A., Izzati, E., 2020. Species composition and habitat preferences of benthic ostracod and foraminifera in seagrass and non-seagrass systems within a tropical estuary. J. Mar. Biol. Assoc. U. K. 100 (8), 1229–1246. https://www.cambridge.org/core/journals/journal-of-the-marine-biological-association-of-the-united-kingdom/article/species-composition-and-habitat-preferences-of-benthic-ostracod-and-foraminifera-in-seagrass-and-nonseagrass-systems-within-a-tropical-estuary/8689448F897DCEC175B1F373880F0F51.

Rijk, S.D., Jorissen, F.J., Rohling, E.J., Troelstra, S.R., 2000. Organic ¯ux control on bathymetric zonation of Mediterranean benthic foraminifera. Mar. Micropaleontol. 16.

Rossbach, F.I., Merk, B., Wild, C., 2021. High diversity and abundance of foraminifera associated with Mediterranean benthic red algae mats. Diversity 14 (1), 21. https://www.mdpi.com/1424-2818/14/1/21.

Schweizer, M., Jauffrais, T., Choquel, C., Méléder, V., Quinchard, S., Geslin, E., 2022. Trophic strategies of intertidal foraminifera explored with single-cell microbiome metabarcoding and morphological methods: what is on the menu? Ecol. Evol. 12 (11), e9437 https://doi.org/10.1002/ece3.9437.

Sen Gupta, B.K., Sen Gupta, B.K., 2003. Introduction to modern foraminifera. In: Modern Foraminifera, pp. 3–6.

Sgarrella, F., Moncharmont Zei, M., 1993. Benthic foraminifera of the Gulf of Naples (Italy): systematics and autoecology. Boll. Soc. Paleontol. Ital. 2.

Swift, D.J.P., Phillips, S., Thorne, J.A., 1992. Sedimentation on continental margins, V: parasequences. Shelf Sand Sandstone Bodies 153–187.

Taviani, M., Vertino, A., López Correa, M., Savini, A., De Mol, B., Remia, A., Montagna, P., Angeletti, L., Zibrowius, H., Alves, T., 2011. Pleistocene to recent scleractinian deep-water corals and coral facies in the Eastern Mediterranean. Facies 57, 579–603.

Tomadin, L., Borsetti, A.M., Cortesogno, L., Franchi, R., Landuzzi, V., Bombardini, L., Mazzuccotelli, A., Oliveti, F., Vannucci, R., Vannucci, S., 1984. Sedimenti Marini Pleistocenico–olocenici in carote del delta padano. Mem. Soc. Geol. Ital. 27, 393–402.

Van der Zwaan, G.J., Duijnstee, I.A.P., den Dulk, M., Ernst, S.R., Jannink, N.T., Kouwenhoven, T.J., 1999. Benthic foraminifers: proxies or problems? A review of paleocological concepts. Earth Sci. Rev. 46, 213–236.

Viola, I., Oppo, D., Franchi, F., Capozzi, R., Dinelli, E., Liverani, B., Taviani, M., 2015. Mineralogy, geochemistry and petrography of methane-derived authigenic carbonates from Enza River, Northern Apennines (Italy). Mar. Pet. Geol. 66, 566–581.

Wang, Z., Pierce, N.E., 2023. Fine-scale genome-wide signature of Pleistocene glaciation in Thitarodes moths (Lepidoptera: Hepialidae), host of Ophiocordyceps fungus in the Hengduan Mountains. Mol. Ecol. 32 (11), 2695–2714.

Wang, P., Tian, J., Lourens, L.J., 2010. Obscuring of long eccentricity cyclicity in Pleistocene oceanic carbon isotope records. Earth Planet. Sci. Lett. 290 (3–4), 319–330.

Woelkerling, W.J., 1988. The Coralline Red Algae: An Analysis of the Genera and Subfamilies of Nongeniculate Corallinaceae. Oxford University Press.

Wollenburg, J., Kuhnt, W., Mackensen, A., 1998. Paleoproductivity of the Arctic Ocean: Evidence by Benthic Foraminifera. International Symposium on Foramininfera. https://epic.awi.de/id/eprint/9806/.

Zattin, M., Picotti, V., Zuffa, G.G., 2002. Fission-track reconstruction of the front of the Northern Apennine thrust wedge and overlying Ligurian unit. Am. J. Sci. 302 (4), 346–379.